applied sciences

MDPI

Article

Dynamic Energy Pricing and Supply–Demand Balancing in a Smart Grid with ANFIS-FOPID Controller: A Comparative Study with PID and FOPID Controllers

Zehva Yalçınöz, Ömerülfaruk Özgüven, Sevgi Gürsul Kalaç and Asım Kaygusuz *

Department of Electrical and Electronic Engineering, Inonu University, 44280 Malatya, Turkey; zehva.yalcinoz@inonu.edu.tr (Z.Y.); omer.ozguven@inonu.edu.tr (Ö.Ö.); sevgi.gursul@inonu.edu.tr (S.G.K.)
* Correspondence: asim.kaygusuz@inonu.edu.tr

Abstract

Renewable energy sources (RESs) enable sustainable and environmentally friendly electricity generation. However, their intermittent nature makes it difficult to maintain energy balance. Smart grids (SGs) address this challenge by enabling grid control under variable demand and fluctuating generation. With the growing share of distributed generation, dynamic energy pricing has become increasingly important for sustaining the supply–demand balance in SGs. This study aims to regulate the interaction between variable demand and distributed generation in SGs using control strategies. The dynamic pricing framework was analyzed using closed-loop Proportional–Integral–Derivative (PID), Fractional-Order PID (FOPID)- and Adaptive Neuro Fuzzy Inference System (ANFIS)-based FOPID controllers. PID and FOPID parameters were tuned by pole placement with reference model matching, while the FOPID parameters in the ANFIS-FOPID structure were adaptively optimized using ANFIS. Energy supply–demand models were developed in MATLAB/Simulink, and the effects of each controller on system dynamics and energy prices were comparatively examined. The results indicate that ANFIS-FOPID achieves lower overshoot, shorter settling time, and more stable balancing performance, owing to its fractional-order flexibility and optimized parameters. In the model established in the MATLAB/Simulink environment, the controllers were evaluated based on integral of squared error (ISE), time-weighted integral absolute error (ITAE), root mean square error (RMSE), average unit energy price, price volatility, and coefficient of variation. A virtual energy storage model was added to the system. Disturbance and load change scenarios were also examined. The results showed that the ANFIS-FOPID controller provided the most balanced performance in terms of error reduction, suppression of price fluctuations, and reduction of the average unit energy price.

Keywords: dynamic energy pricing; renewable energy sources; ANFIS-FOPID; virtual energy storage; distributed generation; supply–demand balancing

Check for updates

Academic Editor: Alessandro Lo Schiavo

Received: 31 March 2026
Revised: 23 April 2026
Accepted: 26 April 2026
Published: 5 May 2026

Copyright: © 2026 by the authors. Licensee MDPI, Basel, Switzerland. This article is an open access article distributed under the terms and conditions of the Creative Commons Attribution (CC BY) license.

1. Introduction

Energy has always been a fundamental human need throughout history. Rising electricity demand, driven by population growth, climate change, and technological progress, has intensified the need for grid resilience with the integration of renewable energy sources (RESs). Increasing consumption also places additional stress on infrastructure. At the same time, efforts to maintain the balance between production and consumption, along

with the pursuit of efficient resource utilization, have increased the demand for flexible control systems. Smart grids (SGs) were developed to modernize conventional power infrastructure and enable the efficient integration of RESs [1]. These advances have reinforced scientific and technical studies in the energy field and brought the sustainable use of energy resources to both national and international agendas [2,3]. As a result, alternative energy management structures such as microgrids and SGs have gained wider adoption.

Energy generation, transmission, and distribution processes must be fast, controllable, and low loss [4]. Interconnected systems consist of long transmission lines, where a single fault can cause large-scale power outages. Conventional grids are often unable to maintain stability under such conditions and fail to meet today's energy requirements. Although traditional grids have advanced in recent years, generation units now reach capacities of several thousand megawatts (MW), while distribution networks still lack advanced automation and real-time monitoring infrastructure. This situation increases security vulnerabilities and limits system flexibility. Accordingly, the need for smart grid (SG) technologies has become more pronounced [5,6]. SGs operate with fully automated control systems, enabling real time monitoring and updating of the grid through smart meters and information technologies [7,8]. Furthermore, automation systems, supported by artificial intelligence and algorithms, help mitigate functional problems of conventional grids and improve overall system efficiency.

Growing energy demand, the limitations of conventional grids, and the environmental and health impacts of fossil fuels are steering the energy sector toward sustainable sources [9]. Excessive reliance on fossil resources poses risks of supply shortages and price increases, while the rise in greenhouse gas emissions drives global warming and climate change. Beyond environmental concerns, the developments of the last five years have made energy security, supply diversification, and infrastructure adequacy central issues in power-system planning [10,11]. In particular, the disruptions experienced during the COVID-19 period, the 2021 gas price shock, and the 2022–2023 Russia–Ukraine-war-related energy crisis clearly demonstrated the economic and operational risks associated with excessive dependence on a limited number of fossil-fuel suppliers [11,12]. For this reason, the recent literature treats renewable energy expansion not only as a decarbonization strategy but also as a means of strengthening energy security, reducing exposure to price volatility, and improving resilience against geopolitical disruptions [10,12]. Moreover, different renewable technologies impose different balancing and transmission requirements because their generation characteristics are not identical; therefore, a diversified portfolio including solar, wind, hydropower, and supportive storage/flexibility options provides a more resilient system structure than dependence on a narrow supply mix [11,13]. From this perspective, the growth of renewable-based power systems should be regarded not as an inevitable future shift, but as an ongoing and accelerating structural transformation [12,13].

RESs, derived from natural processes, offer alternatives to supply imbalances. These resources are inexhaustible due to nature's self-renewal capacity, and their integration reduces dependence on imports and lowers carbon emissions, thereby broadening their applications. Hence, the integration of RESs into power grids must be accelerated and their utilization expanded. However, the intermittent and unpredictable characteristics of these resources introduce operational challenges. The characteristics of electricity generation, the impact on the grid and the installed capacity of renewable energy sources vary. Solar and wind energy generation depends on weather conditions and is therefore variable. This can cause fluctuations in the grid. In contrast, hydroelectric power generation generally provides a more controllable and stable output. Consequently, it contributes more effectively to system balancing. Thermal power generation is more consistent and helps mitigate the fluctuations caused by renewable energy production. Tidal generation is periodic and

depends on regional conditions, which may impose time-dependent production constraints. Effective deployment requires the integration of energy storage systems alongside generation [14]. Peak loads at certain times of the day can create significant pressure on the grid when supply is insufficient [15]. Storage systems address this by capturing surplus or unused energy and feeding it back during high-demand periods. They also mitigate sudden fluctuations in renewable output, thereby enhancing system stability [9,16]. SG structures enable the integration of RES and storage technologies into modern power systems. While conventional sources can respond rapidly to demand variations, renewable output is highly dependent on meteorological conditions. In cases of overproduction, stored energy can be utilized to improve power factor, support system regulation (frequency and voltage), and optimize power flow management [17]. In one study, it was demonstrated that under high RESs penetration scenarios, a balanced mix of solar and wind energy combined with adequate storage capacity provides the most effective solution for minimizing costs and reducing curtailments [18].

The transition to renewable energy sources is being further accelerated by rising energy demand and prices, decarbonization policies, energy security concerns and technological advancements. The aim today is to utilize these energy sources to achieve higher power output and efficiency through various control techniques. These resources transform consumers into producers, reducing demand and contributing to lower energy prices. However, the integration of renewables introduces production fluctuations that diminish the effectiveness of conventional pricing mechanisms. In this context, dynamic energy pricing emerges as a strategic tool to enhance grid flexibility and regulate consumption profiles.

Studies on dynamic energy pricing in the current literature have primarily focused on demand response, RESs integration, and storage-supported SG management. However, in recent years, there has been an increase in forecast-based, market-oriented and optimization-focused studies. Concurrently, the use of meta heuristic optimization methods has grown in order to improve pricing strategies and controller performance. Nevertheless, studies in which the energy price signal is regulated using an adaptive fractional-order controller remain limited. In particular, the integration of the ANFIS-supported FOPID controller into a dynamic energy pricing framework has not yet been adequately investigated in multiple operational scenarios using quantitative performance metrics. This study therefore examines the comparative performance of PID, FOPID and ANFIS-FOPID controllers within a closed-loop dynamic energy pricing framework, with the aim of addressing this gap. The primary objective identified in this context is to ensure supply–demand balance and price stability under various scenarios, such as storage conditions and disturbances.

This study presents a control architecture based on closed-loop dynamic energy pricing and examines the effects of different controller designs on system performance. Energy demand and supply were modeled using hourly data from Turkey. The control signal was generated based on the error between these two variables, and the energy price was dynamically updated. Turkey was selected as the case study country due to the increasing integration of renewable energy sources, the observed growth trends on both the demand and supply sides, and its developing energy infrastructure. The numerical data used in the study were modeled to represent the 24 h characteristics of Turkey's supply and demand curves [19]. Additionally, the method proposed in this study is designed to have a globally applicable structure using demand and supply data from other countries, thereby providing a general framework. In the first phase of the study, a classical PID controller was applied, and the control parameters were determined using the reference model matching method and the pole placement method. Subsequently, the system was tested using a fractional-order PID (FOPID) controller. In this model, the integral and derivative operations were defined in fractional-order form, and the K_p, K_i, and K_d parameters were

calculated using the reference model matching method. In the third stage, the FOPID control parameters were trained using an ANFIS-based learning framework. Adaptive FOPID control parameters were obtained by using the e signal as input for the ANFIS model. This enabled the development of an adaptive controller strategy. A virtual storage system was added to test the system's robustness. The controllers were evaluated under both storage-enabled and storage-less conditions using the integral squared error (ISE), time-weighted integral absolute error (ITAE), root mean square error (RMSE), average unit energy price, price volatility, and coefficient of variation metrics. Additionally, the system's robustness was examined under disturbance and load change scenarios. In this context, the performance of the controller architectures in maintaining supply–demand balance, ensuring price stability, and improving system performance was evaluated comparatively.

Related Work and Main Contributions

Dynamic energy pricing has played a critical role in SG systems, where energy supply and consumption remain balanced. This role is particularly evident in areas targeting real-time demand-side management (DSM), demand response (DR), and the integration of multi-source renewable generation. Recent research has made dynamic pricing an established focus in the literature. Electricity tariffs are typically formed by combining fixed costs from generation, transmission, and distribution with additional charges related to production [20]. These tariffs are classified into simple, flat-rate, block-rate, two-part, and maximum-demand structures. With advancing technology, such schemes have proven inadequate, leading to the development of smart pricing programs. Within DR, these programs are categorized into three main groups: time-of-use (ToU), critical peak pricing (CPP), and real-time pricing (RTP). Their common aim is to influence consumer behavior by adjusting demand in response to dynamic price signals [21]. DSM becomes more effective when supported by price signals [22]. Parvania and Fotuhi emphasized that demand management was decisive in ensuring production consumption balance [23]. The oldest dynamic energy pricing approach is ToU pricing. Due to its simple implementation, ToU has been able to shift peak load by relying on predetermined price levels. However, its ability to reflect market price fluctuations and respond to specific grid conditions has remained limited [24–29]. CPP, which has a simple structure similar to ToU, is implemented within a high rate range during specific time periods [30]. Except for high-cost peak rates, a fixed rate applies throughout the year [31]. Since CPP has covered only certain periods, it has not provided daily variation like other smart pricing schemes [32]. Although CPP has placed greater cost pressure on consumers compared to ToU, both approaches have reduced expenses through load shifting [33]. RTP has been a control mechanism that updates prices continuously based on real-time demand and supply variations. In one study, the effects of the RTP program were examined for two consumer groups, wholesale and retail electricity buyers [34]. In another study, DR benefits were analyzed by constructing real-time RTP models [35,36]. He et al. showed that autonomous and coordinated operation of smart meters reduced peak loads in SG systems [37]. Thus, RTP signals have been an effective strategy in shaping load profiles. However, because consumers cannot regularly follow constantly changing prices and due to infrastructure limitations, RTP has not always delivered the expected outcomes. The main difference among the given pricing schemes has been the variation of costs over the operating period [38].

In today's electricity pricing systems, where structures such as three-time tariffs are applied, dynamic pricing ensures that price levels remain optimal by adapting to changes in demand and generation. This mechanism regulates the effects of rising prices on supply and demand and improves energy efficiency. As a DR-based management method, dynamic pricing aims to reduce peak loads and lower costs by varying prices across dif-

ferent time periods. The approach seeks to balance high production costs during peak hours by shifting load to off peak periods [39]. Most studies in the literature have focused on long- and medium-term forecasting models designed to maximize producer profit. These models have been diversified using methods such as blockchain and artificial neural networks [40,41]. Another study has developed a model redefining producer-consumer interaction with an Arduino-based smart meter, where demand response and pricing were combined [42]. Anand et al. have presented a real-time pricing strategy in a microgrid scenario integrating RES [43]. In another study, dynamic pricing models for SG have been analyzed comparatively using load forecasting and demand-side management techniques [20]. Energy prices rise during peak demand periods due to increased generation. In this context, energy storage systems play a critical role in maintaining supply–demand balance. Their integration into the grid increases the stability of price signals and contributes to real-time balancing processes. Several studies have used storage systems alongside RESs. It has been reported that storage reduces uncertainty in RES output and enhances the effectiveness of pricing strategies [44–46]. Hill et al. have provided a framework for storage technologies used with photovoltaic systems [47]. Owais et al. present an algorithm-based solution for multiple storage systems using load forecasting models and energy prices [48]. Another study introduces a real time pricing method using anti-predatory particle swarm optimization with RES integration and provides comparative results using conventional particle swarm optimization [43].

Recent studies have increasingly integrated dynamic pricing with energy storage coordination, demand response participation, real-time pricing strategies, and optimization-based control structures in smart grids. Meta-heuristic optimization methods, which are also widely used in other data-driven fields such as natural language processing [49], healthcare facility planning, medical image-based diagnosis [50] have been shown to improve controller tuning, operational flexibility, and energy management performance under variable renewable generation and uncertain load conditions [51]. Similarly, evolutionary and bio-inspired optimization approaches combined with FOPID-based structures have provided improved frequency regulation, optimal power flow performance, and more robust control behavior in renewable-integrated power systems [52]. Multi-objective optimization has also gained importance in balancing cost, reliability, storage scheduling, and real-time operational constraints in smart grid applications [53]. In addition, robust control-oriented studies in modern power systems, including HVDC-based applications, further demonstrate the importance of advanced adaptive control structures for maintaining stability under dynamic operating conditions [54]. These developments confirm the need for controller-assisted pricing frameworks that jointly address price stability, supply–demand balancing, and operational robustness in renewable-integrated smart grid environments.

In SGs, dynamic pricing not only enhances flexibility on the demand side but also supports sustainability in generation through closed-loop price control. Regulating energy prices via controllers serves as an example of autonomous energy management in SGs. This approach plays a critical role in maintaining the balance between supply and demand in the energy network. Several studies exist in the literature on optimizing this balance through controller systems. The study conducted by Alagöz et al. introduced the idea of directly regulating energy prices using a PID controller into the literature and was a pioneering work in achieving supply–demand balance. This study demonstrates through simulation that price feedback can improve system stability [55]. This study has formed a reference model in the field of dynamic energy pricing for various works, such as closed-loop super-twisting sliding mode controllers and fractional-order PI [7,56]. In another study, an FOPID controller was developed and combined with the secretary bird algorithm to propose a novel approach for energy management in smart homes [53]. In addition, FOPID

controllers have been extensively examined in the literature across various applications to improve system stability and performance in the energy field. In a study on hybrid generation with storage, an FOPID controller optimized through a genetic algorithm was observed to provide lower frequency deviation and higher stability compared to conventional methods [57]. Many studies have shown that optimized FOPID controller parameters, through their superior and flexible performance, demonstrate the effectiveness of this structure as a control tool [58–61]. Research conducted with controllers shows their effectiveness in regulating energy prices and balancing consumption with supply. It has been emphasized that ANFIS can optimize power sharing among multiple energy sources in a micro grid environment [62]. Islam et al. showed that the same method produced successful results in battery management systems [63]. The ability of ANFIS to adaptively learn control parameters makes it suitable for error-based optimization scenarios [64]. Several studies have highlighted that AI-based controllers such as ANFIS provide resilience against uncertainty in market conditions [65,66].

Hybrid approaches based on ANFIS have gained prominence by integrating multiple methods to achieve higher accuracy. Wu et al. developed a hybrid model for short-term load forecasting by combining the ANFIS structure with the Elman neural network (ELM). In this model, the weight coefficients were optimized using an improved parasitism–predation algorithm, and simulation results demonstrated superior performance compared with ELM, ANFIS, and other state-of-the-art techniques [67]. In another study, a hybrid ANFIS–genetic algorithm (ANFIS-GA) approach was proposed for ventilation systems in underground mines, where model structure optimization yielded higher accuracy in airflow and energy consumption prediction compared with several alternative methods. The study reported low root mean square error (RMSE) and mean absolute error (MAE) values, indicating that ANFIS-GA is a safe, efficient, and applicable method [68]. Similarly, in a separate study conducted for a wind farm in Brazil, various machine learning algorithms were developed for time-series wind speed prediction. Tests at different time intervals showed that optimizing ANFIS with particle swarm optimization (PSO) and GA significantly improved prediction accuracy [69].

The optimization of FOPID controller parameters with ANFIS is widely applied in applications requiring high stability and flexibility. In one study, an ANFIS-FOPID structure was used for maximum power point (MPP) tracking and provided higher efficiency and stability compared with existing methods [70]. A similar study used an ANFIS-FOPID controller to determine the maximum power voltage error in MPP tracking [71]. Another study applied an ANFIS-FOPID structure to battery charging systems in electric vehicles [72].

In this context, the absence of an ANFIS-FOPID application integrated into dynamic energy pricing in the existing literature increases the originality of the present study. The proposed model minimizes price fluctuations, maintains supply–demand balance in a stable manner, and reduces the average price level, thereby making a significant contribution to the literature. This work offers a distinct solution by addressing price fluctuation reduction in energy markets through the integration of classical methods with the AI-based optimization approach of ANFIS-FOPID, thereby setting it apart from related studies.

This study has been designed to complement existing research and achieve the specific objectives outlined below:

1. Evaluate the comparative performance of PID, FOPID and ANFIS-FOPID controllers under the same operating conditions within a closed-loop dynamic energy pricing structure.
2. Examine controller performance in detail using quantitative metrics such as error measures (ISE, ITAE, and RMSE) and price-related criteria.
3. Demonstrate the impact of controller behavior on the balance between supply and demand and price stability under both storage-based and non-storage-based scenarios.

4. Test the system's robustness and performance under disturbance and load change scenarios.

Although this study focuses primarily on the performance of the control device, a more predictable pricing structure for consumers may be achieved indirectly through a reduction in price volatility.

The remainder of this paper is organized as follows. Section 2 presents the methodology of the control approaches employed. Section 3 introduces the dynamic energy pricing structure together with its mathematical model and supply–demand-based formulations. Section 4 compares the simulation results obtained under different scenarios. Section 5 presents the results and discussion. Finally, Section 6 concludes the paper.

2. Methodology

In system analysis, the clear definition of objectives is of critical importance. The primary goal in control system design is to obtain an output that satisfies the specified performance criteria in response to the input signal [73]. Accordingly, the output is expected to follow the input rapidly, accurately, and with minimal distortion. System performance is evaluated in line with the design criteria and must remain consistent with the computational process. Control systems can be designed through structures such as input–output representation, time–frequency response, and transfer function.

Different methods are used in control system design. Among the most common approaches are closed loop Ziegler-Nichols, open-loop Cohen-Coon, and pole placement techniques [8,74–76]. The common objective of these methods is to obtain control parameters as efficiently as possible. In particular, the pole-placement method allows system stability to be examined by positioning poles within target regions. In the literature, this method is widely applied [77–79].

This study presents a comparative analysis of PID, FOPID, and ANFIS-FOPID controllers. The system methodology consists of the steps outlined below.

2.1. Dynamic Energy Price System Design

Controllers are fundamental components of a control system and ensure that the output signal is produced in a stable, rapid, and distortion-free manner according to the input signal. Figure 1 illustrates the structure of a typical control system. Here, $r(t)$ denotes the reference input, $e(t)$ denotes the error, $u(t)$ denotes the control variable applied to the system input, and $y(t)$ denotes the system output. The error is defined as the difference between the reference input and the system output.

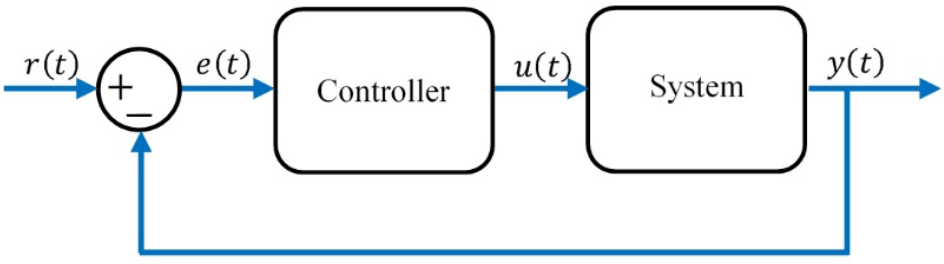


Figure 1. Block diagram of a basic feedback control system (prepared by the authors).

The error obtained from the difference between demand and supply, as shown in Figure 1, is processed through the PID, FOPID, and ANFIS-FOPID controllers, respectively, and a dynamic price signal is generated to ensure system stability.

Figure 2 presents the Simulink model of the dynamic pricing system. The difference between demand and supply is defined as the error signal, which is applied to the PID, FOPID, and ANFIS-FOPID controllers, respectively. Switches Sw1 and Sw2 enable tran-

sitions between the controllers. The controller outputs generate the energy price signal, allowing direct performance comparison. Considering variations in supply and demand, the price signal is updated dynamically. Through this Simulink model, the dynamic pricing performance of different controllers is evaluated under a common framework.

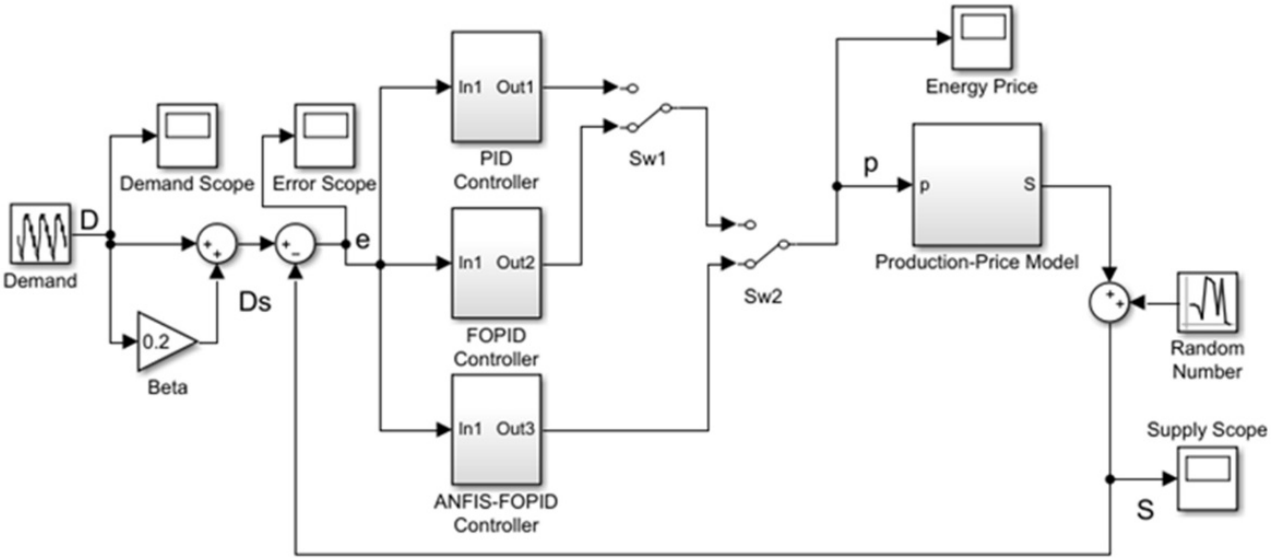


Figure 2. General Simulink model of the dynamic energy pricing structure (authors' own work).

2.1.1. PID Controller

One of the controllers used in this study is based on the Proportional–Integral–Derivative (PID) structure, which is widely applied in the literature. A PID controller consists of proportional (K_p), integral (K_i), and derivative (K_d) components. Proportional control applies a correction proportional to the current error, while integral control eliminates the steady-state error and operates independently of system gain. Derivative control aims to counteract potential future deviations by responding to the rate of change of the error. The combination of these three actions seeks to minimize system error by reacting to past, present, and anticipated error trends [80,81]. The error signal, which serves as the input to the PID controller, is processed until the reference output is achieved. The performance of the PID controller varies depending on the accuracy of its parameters [82,83]. Numerous studies have been conducted on accurate parameter estimation [74,76,84].

The transfer function of the first-order system with a PID controller in the s-domain is given in Equation (1) [75].

$$G_{PID}(s) = \frac{U(s)}{E(s)} = K_p + \frac{K_i}{s} + K_d s \quad (1)$$

Figure 3 illustrates the internal structure of the PID controller used in the general model presented in Figure 2. The gains K_p, K_i, and K_d are defined as separate blocks. The error signal is applied to these blocks, and the resulting outputs are summed to generate the controller output. This configuration has been employed as a reference control method to examine the fundamental behavior of the system.

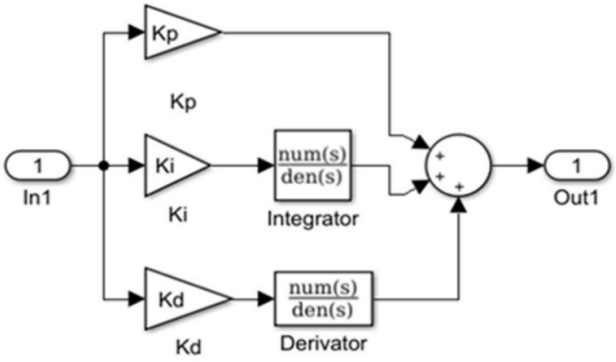


Figure 3. Simulink model of the PID controller structure (authors' own work).

2.1.2. FOPID Controller

The FOPID controller, as an extension of the PID structure, defines the integral and derivative terms at fractional orders. This structure expands the memory effect of the controller and enables a more detailed evaluation of past system behavior. The FOPID controller includes not only the coefficients, K_p, K_i, and K_d, but also the parameters λ (integral order) and μ (derivative order). In this way, it manages time-dependent system dynamics more flexibly. Widely applied in many fields, the FOPID controller has become an active area of research in the literature [53,85–90]. Especially in uncertain or nonlinear systems, FOPID offers better transient and steady-state responses compared with the classical PID controller. Therefore, the FOPID controller improves system performance relative to the PID controller [91].

The transfer function of the first-order system with a FOPID controller in the s-domain is given in Equation (2) [92].

$$G_{FOPID}(s) = \frac{U(s)}{E(s)} = K_p + \frac{K_i}{s^{\lambda}} + K_d s^{\mu} \quad (2)$$

Figure 4 presents the detailed Simulink representation of the FOPID controller integrated into the general model of Figure 2. The K_p, K_i, and K_d gains are defined as separate blocks. The integral and derivative components are modeled as fractional-order structures. The error signal is applied to these blocks, and the resulting outputs are summed to obtain the controller output. Compared with the classical PID controller, this structure provides greater flexibility in parameter adjustment through the λ and μ derivative orders.

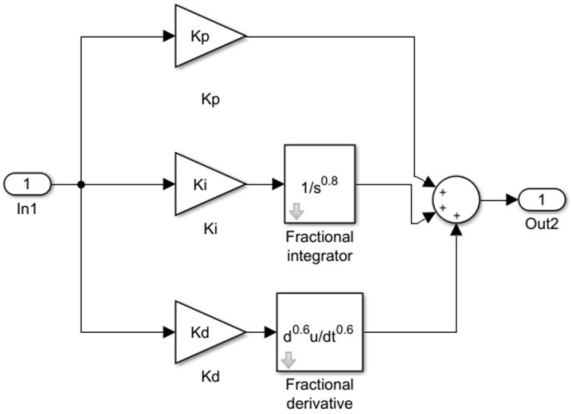


Figure 4. Simulink model of the FOPID controller structure (authors' own work).

2.2. ANFIS Structure

The ANFIS architecture structurally consists of antecedent and consequent components. The training of the model involves determining the parameters of these components through an appropriate optimization method. For training, the input and output data of the system are used as a basis. Based on these data, fuzzy if–then rules that establish relationships between the antecedent and consequent layers are automatically derived [93,94]. The fuzzy rules of a controller with two input variables and one output variable are defined in Equation (3) [90]:

$$\begin{array}{l} \text{Rule 1: if } x_1 = A_1 \text{ and } x_2 = B_1 \text{ then } z = C_1 \\ \text{Rule 2: if } x_1 = A_2 \text{ and } x_2 = B_2 \text{ then } z = C_2 \end{array} \tag{3}$$

Here, A_1, A_2, B_1, and B_2 represent the membership functions of the input variables (antecedent part), while C_1 and C_2 denote the membership functions of the output variable (consequent part). Another alternative representation was developed by Takagi and Sugeno, in which the input variables are defined by membership functions, whereas the output is expressed through linear mathematical equations [95]. According to the Takagi–Sugeno approach, the rule structure of a system with two input variables, one output variable, and two rules can be expressed as follows:

$$\begin{array}{l} \text{Rule 1: if } x_1 \text{ is } A_1(x_1) \text{ and } x_2 \text{ is } B_1(x_1) \text{ then } f_1(x_1, x_2) = p_1 x_1 + q_1 x_2 + z_1 \\ \text{Rule 2: if } x_1 \text{ is } A_2(x_1) \text{ and } x_2 \text{ is } B_2(x_2) \text{ then } f_2(x_1, x_2) = p_2 x_1 + q_2 x_2 + z_2 \end{array} \tag{4}$$

For a single-input (e) system with n rules and $p_i = q_i = 0$ $(i = 1, \cdots, n)$, the rules can be rewritten as follows:

$$\begin{array}{ll} \text{Rule 1} & \text{if error} = A_1(e) \text{ then } f_1(e) = z_1 \\ \text{Rule 2} & \text{if error} = A_2(e) \text{ then } f_2(e) = z_2 \\ \vdots & \vdots \\ \text{Rule } n & \text{if error} = A_n(e) \text{ then } f_n(e) = z_n \end{array} \tag{5}$$

The ANFIS structure shown in Figure 5 consists of five layers. Here, A_1, A_2, $\cdots$, A_n, represent the positions of the membership functions, while z_1, z_2, $\cdots$, z_n denote the output function parameters determined through the training process.

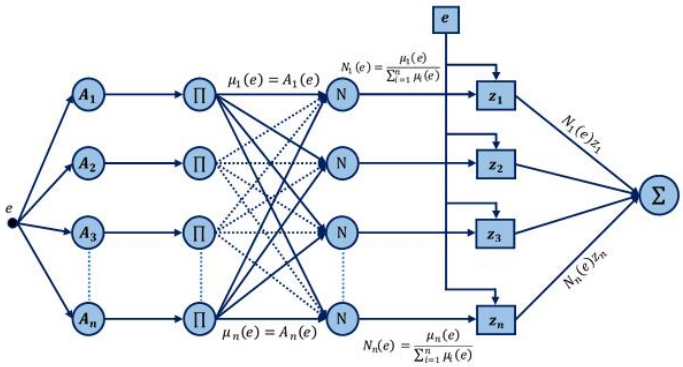


Figure 5. The ANFIS structure with one input and one output (redrawn from [90]).

The first layer is called the fuzzification layer. Membership functions are used to obtain fuzzy sets from the input values. The parameters that determine the shape of the membership functions are defined as antecedent parameters. Each node can use such fuzzy membership functions in the form of $A_i(e)$.

The second layer is called the rule layer. The inference obtained using the rules is calculated based on the membership values derived in the fuzzification layer and is given in Equation (6).

$$\mu_{A_1} = A_1(e),\ \ \mu_{A_2} = A_2(e), \cdots, \mu_{A_n} = A_n(e) \tag{6}$$

The third layer is called the normalization layer. In this layer, each node calculates its normalized weight by dividing its own firing strength by the total firing strength of all rules. The normalized weights are given in Equation (7).

$$\begin{aligned} N_1(e) &= \frac{\mu_{A_1}}{\mu_{A_1}+\mu_{A_2}+\cdots+\mu_{A_n}} \\ N_2(e) &= \frac{\mu_{A_2}}{\mu_{A_1}+\mu_{A_2}+\cdots+\mu_{A_n}} \\ &\vdots \\ N_n(e) &= \frac{\mu_{A_n}}{\mu_{A_1}+\mu_{A_2}+\cdots+\mu_{A_n}} \end{aligned} \tag{7}$$

The fourth layer is called the consequent layer, and for each node (i), it applies the operations given in Equation (8).

$$f_1(e) = z_1,\ f_2(e) = z_2,\ \cdots, f_n(e) = z_n \tag{8}$$

The fifth layer, the output layer, is called the summation layer. The final output of ANFIS is calculated as the sum of the outputs corresponding to each rule. It is the total of the signals transmitted from the consequent layer.

$$y(e) = N_1(e)\cdot f_1(e) + N_2(e)\cdot f_2(e) + \cdots + N_n(e)\cdot f_n(e) \tag{9}$$

$$y(e) = \sum_{i=1}^{n} N_i(e)\cdot f_i(e) \tag{10}$$

$$y(e) = \frac{\sum_{i=1}^{n} \mu_i(e)\cdot f_i(e)}{\sum_{i=1}^{n} \mu_i(e)} = \frac{\sum_{i=1}^{n} A_i(e)\cdot f_i(e)}{\sum_{i=1}^{n} A_i(e)} \tag{11}$$

The training of ANFIS refers to determining structural parameters through an optimization algorithm. In this process, both antecedent and consequent parameters are used. For effective outcomes, successful training of the model is of critical importance. Since the development of ANFIS, various training methods aimed at improving its performance have been proposed. These methods are classified into three groups: derivative-based, heuristic-based, and hybrid approaches.

2.3. ANFIS-FOPID Controller Systems

Figure 6 presents the structure in which the FOPID controller parameters (K_p, K_i, and K_d) are tuned using ANFIS.

As shown in Figure 6, the difference between the input and output of the FOPID-controlled system is the error signal.

$$e(t) = r(t) - y(t) \tag{12}$$

The controller coefficients of the FOPID-controlled system are obtained using Equation (13).

$$\begin{aligned} K_p(e) &= \frac{\sum_{i=1}^{n} A_i(e)\cdot f_i(e)}{\sum_{i=1}^{n} A_i(e)} \\ K_i(e) &= \frac{\sum_{j=1}^{m} B_j(e)\cdot f_j(e)}{\sum_{j=1}^{m} B_j(e)} \\ K_d(e) &= \frac{\sum_{k=1}^{v} C_k(e)\cdot f_k(e)}{\sum_{k=1}^{v} C_k(e)} \end{aligned} \tag{13}$$

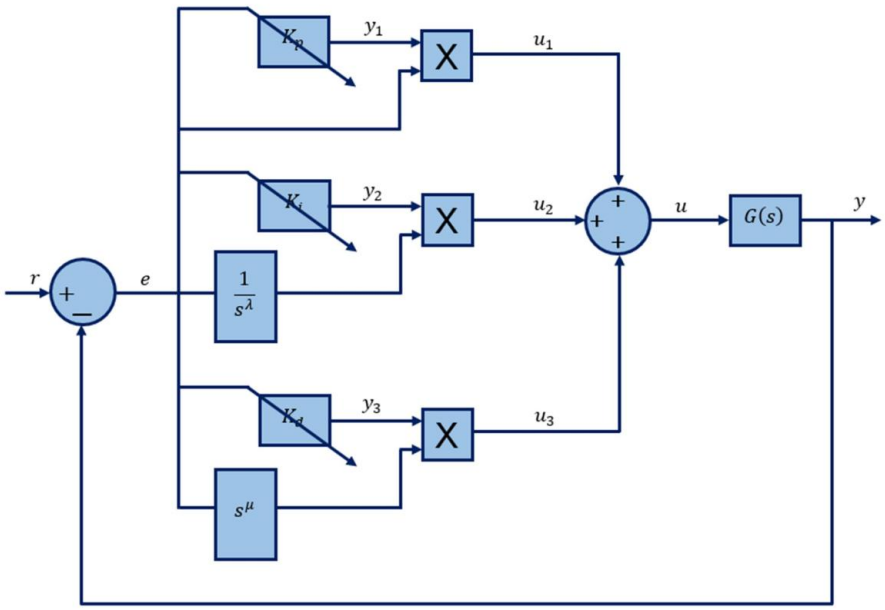


Figure 6. Block diagram of the adaptive FOPID controller (redrawn from [90]).

For the expression given in Equation (13), $A_i(e)$, $f_i(e)$, $B_j(e)$, $f_j(e)$, $C_k(e)$, $f_k(e)$ represent the membership and output functions of all rules corresponding to K_p, K_i, and K_d, respectively. Thus, if the block diagram presented in Figure 6 is rewritten by substituting the expressions given in Equation (13), it is illustrated in Figure 7.

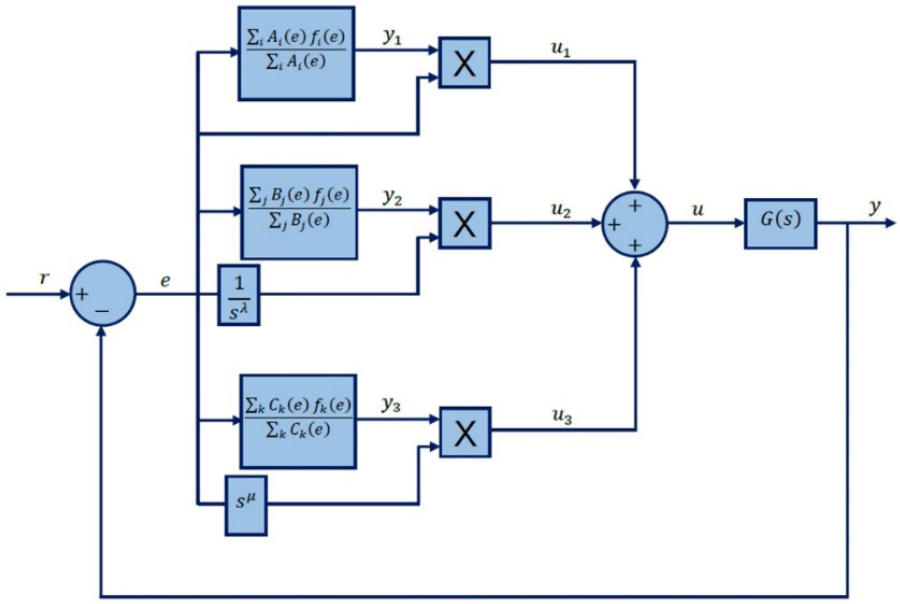


Figure 7. Block diagram of the adaptive FOPID controller modeled with ANFIS (redrawn from [90]).

Figure 8 illustrates the detailed Simulink representation of the ANFIS-FOPID controller within the general model presented in Figure 2. Gains K_p, K_i, and K_d were initially taken as the values calculated for the FOPID controller. The integral and derivative terms are modeled as fractional-order components. The error signal enters these blocks, and the controller produces the energy price signal at its output. This model adaptively adjusts the parameters, providing a more flexible control structure.

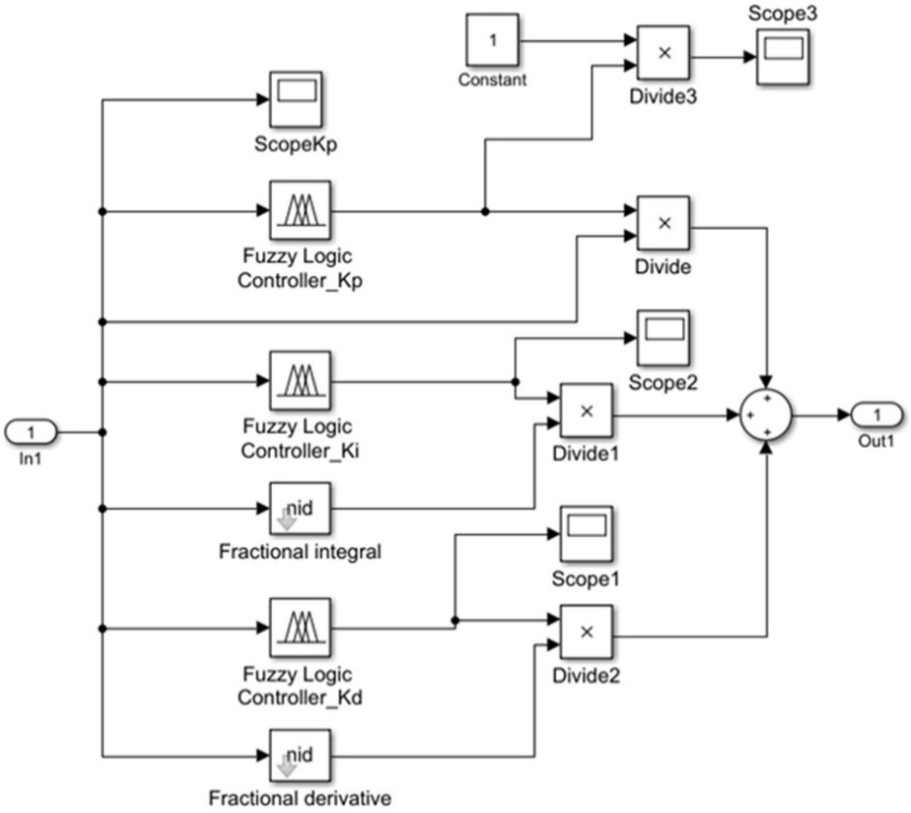


Figure 8. Simulink model of the ANFIS-FOPID controller structure (authors' own work).

In this study, as shown in Figure 9, a Sugeno-type ANFIS model was developed for the K_p, K_i, and K_d parameters within the ANFIS-FOPID architecture. The same ANFIS structure was used separately for each of the three control parameters. The same model structure was implemented as separate ANFIS blocks for each of the three parameters. Each model has a single input and a single output. The input variable is the error signal, and the output variable is the corresponding control parameter. The initial FIS structure was created using the grid partition method, and 35 input membership functions and 35 fuzzy rules were used in each model. The input membership functions were selected as gbellmf. The training data were obtained from the FOPID system implemented in the MATLAB/Simulink R2017a environment. In the Simulink structure shown in Figure 10, the error signal was matched with the corresponding control loop outputs; data pairs numbered x_1-u_1, x_2-u_2, and x_3-u_3 were created for training the K_p, K_i, and K_d parameters, respectively. These data pairs were saved as files and trained using a hybrid learning algorithm. At the end of the training process, FIS files were obtained for the relevant ANFIS structures. Testing the training data revealed that the error value was quite low. Figure 11 presents a comparative display of the ANFIS model's training data and the FIS output for the K_p, K_i, and K_d parameters. This structure ensured that the training process was set up in a numerically traceable and repeatable manner.

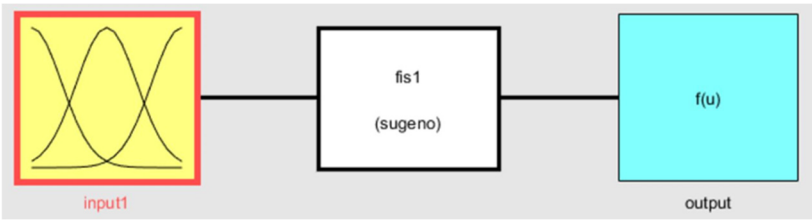


Figure 9. The ANFIS architecture created for the controller parameters (authors' own work).

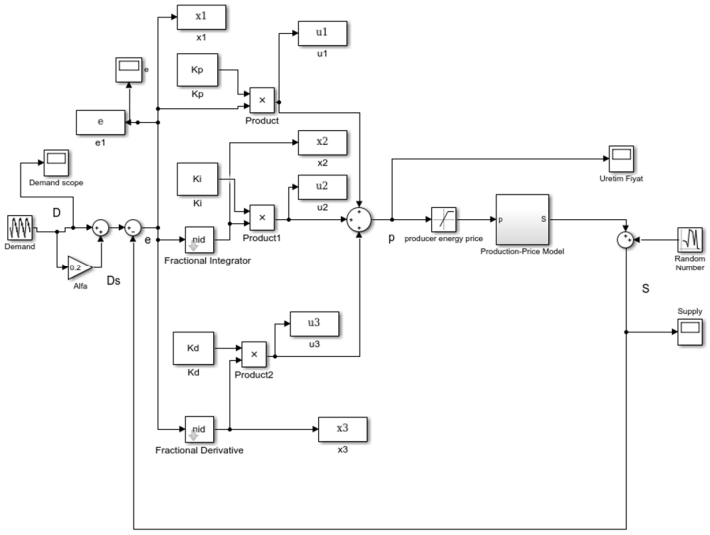


Figure 10. The FOPID-based Simulink model used to generate ANFIS training data pairs parameters (authors' own work).

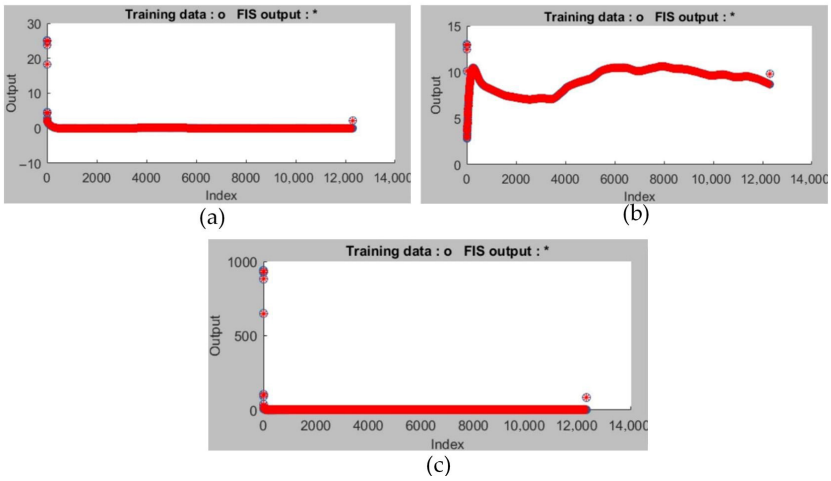


Figure 11. Comparison of training data with FIS output for ANFIS models: (**a**) K_p, (**b**) K_i, (**c**) K_d (authors' own work).

Using the Simulink structure shown in Figure 10, the control loop outputs were matched with the error signal. Through this structure, data pairs x_1-u_1, x_2-u_2, and x_3-u_3 were generated for the parameters K_p, K_i, and K_d respectively, and were used in the ANFIS training.

The results obtained during the testing process indicate that the error value remained at a very low level. Figure 11 presents a comparative display of the training data for the ANFIS model and the FIS output.

As shown in Figure 11, the ANFIS outputs for the parameters K_p, K_i, and K_d exhibit a high degree of agreement with the training data. The results demonstrate that the ANFIS models successfully learned the relevant parameter variations.

3. Dynamic Energy Pricing—Controlled System Model and Formulation

3.1. Closed Loop Control Structure

In pricing dynamics, supply and demand data are the two variables of central importance. Figure 12 illustrates the equilibrium point in product pricing, which occurs at the intersection of the supply and demand curves. Here, 'D' represents the demand function, 'S' represents the supply function, 'N' represents the product quantity, 'p' represents the price, and point 'Q' represents the equilibrium price. A decrease in energy prices leads to

reduced supply and increased demand, while an increase in energy prices restricts demand and encourages supply [55].

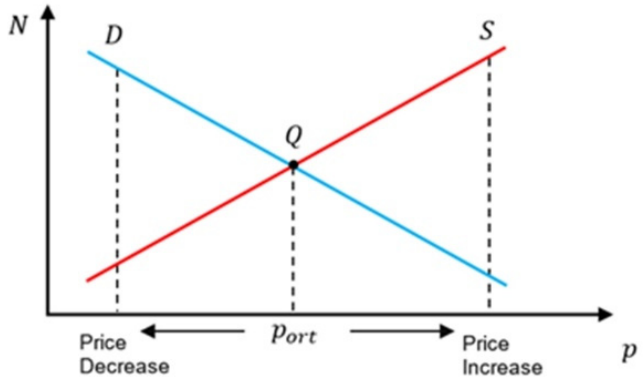


Figure 12. Relationship between demand and supply (redrawn from [55]).

The function e represents the difference between demand and supply and is referred to as the error signal. At point Q, this difference equals zero, which constitutes the optimal price point. Based on the error signal function e defined in Equation (14), the PID, FOPID, and ANFIS-FOPID controllers are activated. According to this equation, the optimal point in dynamic pricing curves is determined as the condition where supply and demand are equal.

$$e = D - S \tag{14}$$

If the error signal function e is greater than zero ($e > 0, \ D > S$), the total production is smaller than the demand volume. In this case, since production cannot meet demand, an energy shortage referred to as energy scarcity occurs. When the error signal e is less than zero ($e < 0, \ D < S$) , the production volume exceeds demand. This situation leads to energy inefficiency due to overproduction and unused capacity. For varying demand values, e is driven toward zero so that balance can be established between supply and demand. In the simulations, to counter the case of $e > 0$ and to prevent energy scarcity by ensuring production remains above demand, a virtual demand term (D_S) is employed [8,55]. Virtual demand is used to trigger production. Accordingly, the e function must be reformulated. If $D_S = \beta \cdot D$, then β represents the virtual demand ratio applied under energy scarcity conditions. For the simulations conducted, the virtual demand ratio was taken as 0.2. Equations (15) and (16) are obtained by reformulating the error signal function with virtual demand.

$$e = D + D_S - S \tag{15}$$

$$e = D + \beta \cdot D - S = D \cdot (\beta + 1) - S \tag{16}$$

In this study, which aims to maintain the equilibrium energy price under variable demand and uncertain production conditions, the input to the PID, FOPID, and ANFIS-FOPID controllers is the error signal e, while the output is the energy price signal p. The controller regulates the error signal e to bring production and consumption data closer together. The price signal obtained at the point where production and consumption converge most closely represents the optimal unit energy price. In dynamic pricing systems with PID, FOPID, and ANFIS-FOPID control mechanisms, production is optimized by adjusting the price signals to adapt to variable demand data.

In studies dependent on energy prices, the accurate calculation of controller parameters is required to ensure the effective execution of the simulation work. For this purpose, the mathematical model of the energy production system used in the simulation must be

formulated in accordance with the system. The energy production model applied to the system is given in Equation (17), where the price responses of energy producers are analytically represented [8,55].

$$S_d(p) = \sum_{i=0}^{d} a_i \cdot p^i \quad (17)$$

Here, d is the degree of the polynomial, and a_i are the polynomial coefficients. According to this model, an increase in the unit energy price results in a rise in production quantity. To complete the production modeling, the delay arising from the producer community must be considered. For this purpose, a capacitive delay model has been selected in accordance with the transfer function in the s-domain to represent this delay. In this production model, τ is the time constant, which denotes the time delay caused by the producer community in response to demand. The energy production volume model, established by considering this production delay, is given in Equation (18) [55].

$$S = S_d(p) \cdot \frac{1}{\tau s + 1} \quad (18)$$

The polynomial $S_d(p)$ characterizes the instantaneous energy selling tendency of producers. This polynomial directly affects the gain of the first-order dynamic system model, namely the coefficient K in the transfer function. For a system whose transfer function is given by Equation (19), if $K = S_d(p)$, as derived above, a higher energy price yields a larger value of $S_d(p)$. Consequently, this increases the gain K, which implies that producers sell energy more quickly and strongly.

$$G(s) = \frac{K}{\tau \cdot s + 1} \quad (19)$$

The system dynamics are modeled by the transfer function expressed in Equation (20).

$$H(s) = \frac{1}{\tau s + 1} \quad (20)$$

Demand response methods can be used in SGs to prevent fluctuations in energy prices [96]. In this way, with price updates taken at short time intervals, energy production and consumption can be controlled. As a result, efficiency in energy is achieved and balance is maintained.

3.2. Simulation Study of Dynamic Price Control in an Energy Network Using Renewable Energy Sources

With the effective use of RESs and the integration of their output with that of other sources, both production efficiency is achieved and the use of environmentally harmful fossil fuels is reduced. In the simulation scenario used in this study, with an installed capacity of 53 MW, the total generation obtained from thermal, hydroelectric, solar, wind, and tidal energy is analytically modeled as shown in Equation (21). In this equation, m denotes the number of resource types, while G_i represents the total amount of energy produced by the i-th source. The total generation from all sources is represented by S_T.

$$S_T = \sum_{i=1}^{m} G_i \quad (21)$$

The production models developed by considering the natural characteristics of each generation source, along with their maximum capacities and production delays within the system, are presented in detail in Table 1.

Table 1. Parameters used for the generation scenario by resource type (adapted from [55], with the tidal source added by the authors).

Resource Type	C_{max} (MW)	Time Constant (h)	Generation Model
Thermal	10	0.31	$\frac{0.01p^2+2.5p}{0.31s+1}$
Hydropower	30	0.052	$\frac{0.01p^2+2.5p}{0.052s+1}$
Wind	6	0.084	$\frac{0.01p^2+2.5p}{0.084s+1}$
Solar	4	0.052	$\frac{0.01p^2+2.5p}{0.052s+1}$
Tidal	3	0.07	$\frac{0.01p^2+2.5p}{0.07s+1}$

Figure 13 shows a Simulink model of multiple energy sources representing the price-production structure within the general model presented in Figure 2. Thermal, hydroelectric, wind, solar, and tidal power plants are defined as separate blocks. The generation profile of each source is modeled using relevant functions, and the supply signal is derived from the sum of these sources. A storage block, which can be activated by a manual switch, is incorporated into the structure, allowing its impact on supply continuity to be examined. This design enables the analysis of the dynamic response of the pricing mechanism under different generation scenarios. Figure 14 shows the output responses obtained from this system.

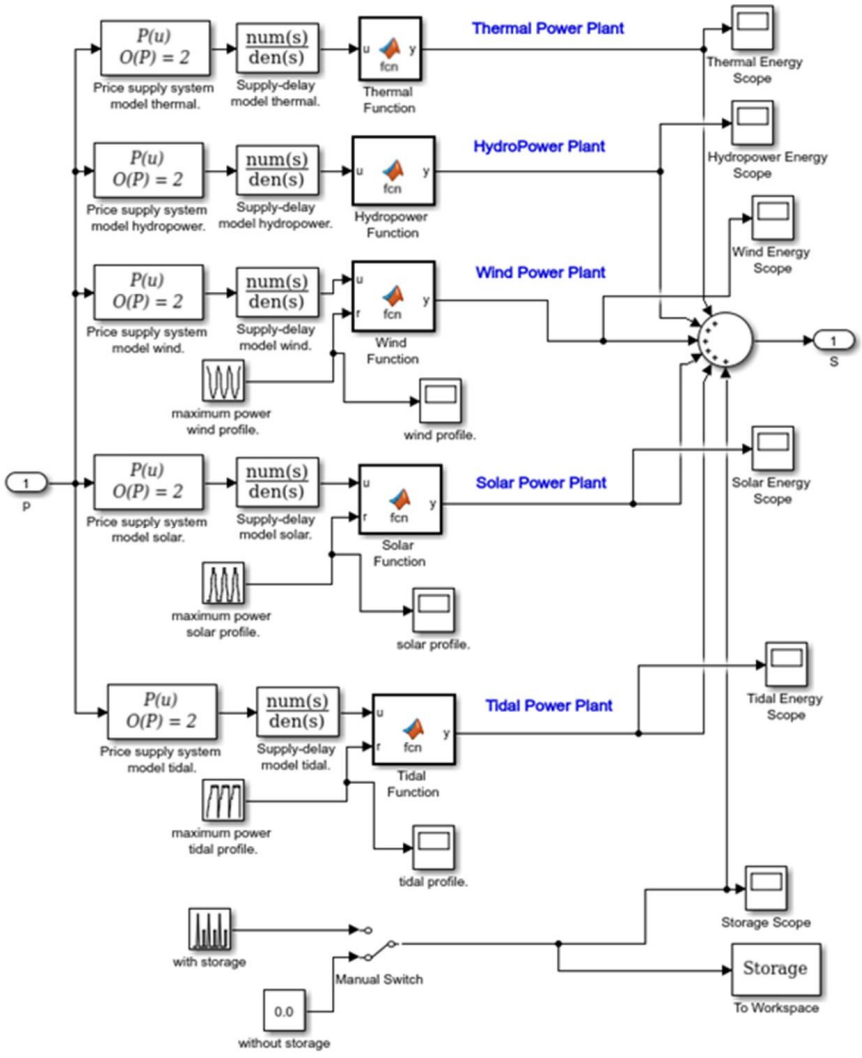


Figure 13. Supply model including multiple energy production sources (Thermal, Hydro, Wind, Solar, Tidal) and storage block (authors' own work).

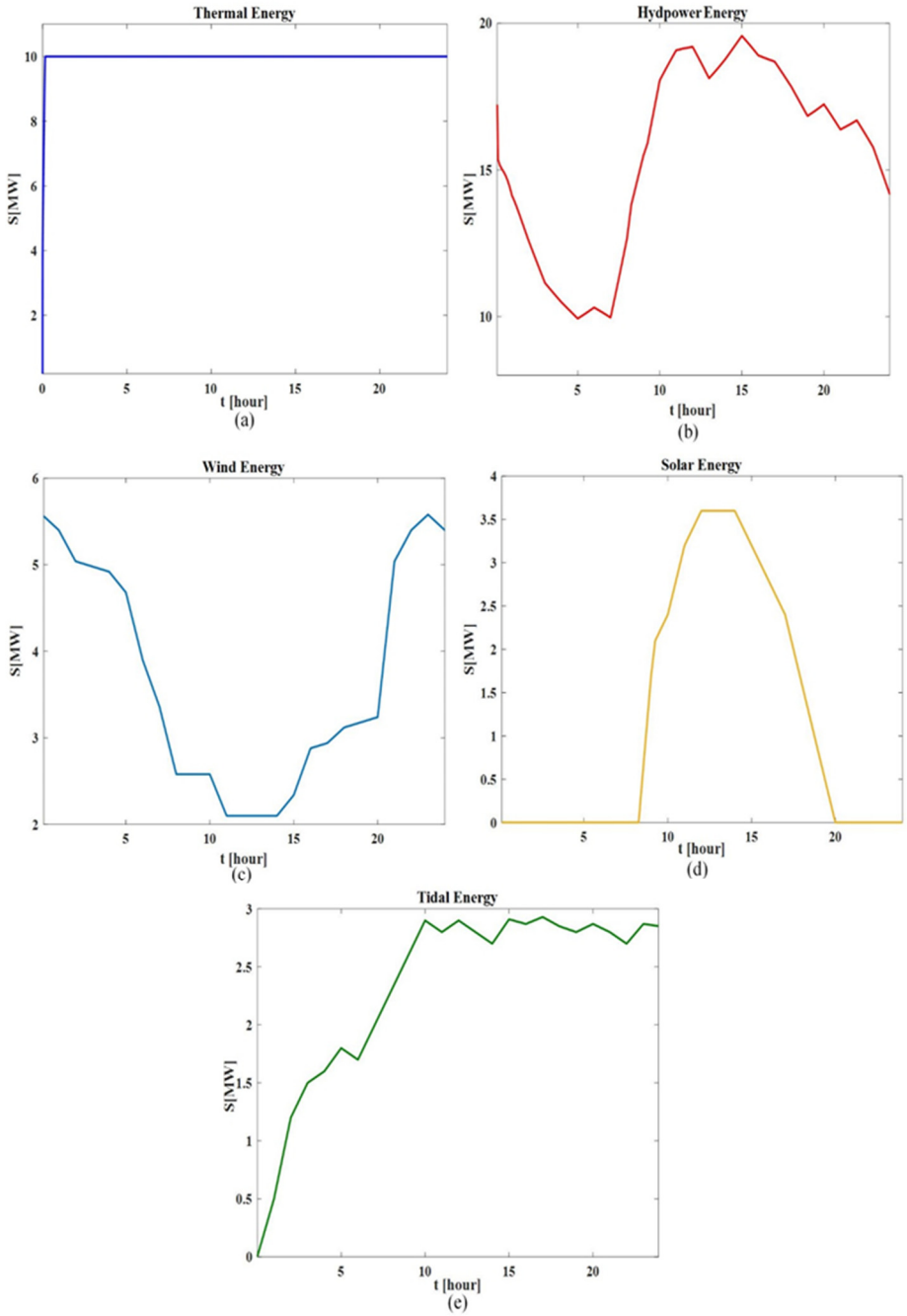


Figure 14. Models of multi-source energy production structures: (**a**) thermal energy, (**b**) hydropower energy, (**c**) wind energy, (**d**) solar energy, (**e**) tidal energy (authors' own work).

Within RESs, fluctuating generation exists, and these sources may cause uncertainty in production. The generation graphs are obtained using the mathematical equations provided in Table 1. As shown in Figure 14, thermal sources maintain stable and uninterrupted generation throughout the day, while solar, wind, hydroelectric, and tidal energy sources exhibit variability. Solar generation increases in the morning, peaks at noon, and drops to zero in the evening. Wind generation is high during the morning and night but low at midday. The thermal plant produces a constant 10 MW throughout the day, representing continuous generation capacity used to balance the fluctuations caused by RESs. Hydroelectric production operates flexibly during the day to compensate for renewable generation variability. Tidal generation rises gradually from the early hours of the day and, after approximately the 10th hour, shows a more stable production profile.

3.3. Computation of Controller Parameters Based on Pole Placement Method with Reference Model Matching

One of the fundamental methods used in control system design, the pole placement method, has been addressed in the literature with various application approaches. In this method, by placing the poles at desired locations, the system can be computed in accordance with the specified criteria. In this study, closed-loop energy price control was examined to ensure a balance between energy supply and demand. The smart grid structure plays a critical role in implementing this control, as it transmits supply and demand signals to the controller through sensors and receivers, thereby guiding the price determination process. For this purpose, a first-order system was considered, and the controller system parameters were determined using the pole placement method based on reference model matching. In the pole placement process, the system poles were obtained from the roots of the characteristic equation using the constant damping ratio (ζ) and natural frequency (ω_n). These roots were then substituted into the characteristic equation of the closed-loop transfer function, thereby defining the system model. Accordingly, PID- and FOPID-based control parameters were calculated, and the design was carried out. Stability analysis was performed for each time interval, and based on the obtained parameters, 24 h dynamic price curves were generated.

For the 53 MW system examined with the integration of RESs, accurate computation of controller coefficients is required to ensure effective and reliable simulation performance. In our previous study, the pole placement method was applied, and the variation of the natural frequency (ω_n) was used to calculate the necessary parameters for the system [97]. In this study, the most suitable values of ω_n and damping ratio (ζ) were determined based on the earlier work. Accordingly, ω_n was set to 4 rad/s. The damping ratio ζ is a key parameter used to assess system stability, as it shifts the pole locations of the system. It represents the degree of oscillation damping and plays a significant role in stability analysis. For $0 < \zeta < 1$, the closed-loop poles are conjugate, lie in the left half-plane, and the system is underdamped [75]. Therefore, the damping ratio ζ was taken as 0.7.

3.3.1. Determination of PID Control Parameters Using Reference-Model-Based Pole Placement

The transfer function of the PID controller is given in Equation (1), while $H(s)$ is defined by Equation (20). When the PID controller is used in the system shown in Figure 1, the closed-loop transfer function of the system, $T(s)$, is expressed in Equation (22).

$$T(s) = \frac{G_{PID}(s) \cdot H(s)}{1 + G_{PID}(s) \cdot H(s)} \tag{22}$$

When the functions given in Equations (1) and (20) are substituted into Equation (22), $T_1(s)$ is expressed in Equation (23).

$$T_1(s) = \frac{K_d \cdot s^2 + K_p \cdot s + K_i}{(K_d + \tau) \cdot s^2 + (K_p + 1) \cdot s + K_i} \tag{23}$$

When the denominator of Equation (23) is equated with the characteristic equation, Equation (24) is used to calculate the controller parameters of the system.

$$\Delta = s^2 + 2 \cdot \zeta \cdot \omega_n \cdot s + {\omega_n}^2 = (K_d + \tau) \cdot s^2 + (K_p + 1) \cdot s + K_i \tag{24}$$

By setting the first term in Equation (24) equal to zero and substituting the specified values $\omega_n = 4$ rad/s and $\zeta = 0.7$, one root of the system is obtained as $s_1 = -2.8 + j2.8566$.

This root can be expressed in polar form as $s_1 = 4\angle 2.3462^r$. The s^2 and s terms specified in Equation (24) are analytically derived in Equation (25).

$$\begin{aligned} s^2 &= -4.4799 - j15.36 \\ s_1 = s &= -2.8 + j2.8566 \end{aligned} \tag{25}$$

By substituting the obtained s^2 and s root expressions, the equation is separated into two components: the real and imaginary parts. These two components are analytically given in Equation (26).

$$\begin{aligned} real &= -4.4799K_d - 1.38878 - 2.4K_p + K_i \\ imaginary &= -15.36K_d - 1.5616 + 3.2K_p \end{aligned} \tag{26}$$

By setting the real and imaginary parts equal to zero and solving, the expressions of each equation in terms of K_i are presented in Equations (27) and (28), respectively.

$$K_d = 0.0625K_i - 0.31 \tag{27}$$

$$K_p = 0.35K_i - 1 \tag{28}$$

3.3.2. Design of the FOPID Controller: Extended Pole Placement and Parameter Tuning

The transfer function of the FOPID controller is defined in Equation (2). When the FOPID controller is used in the system shown in Figure 1, the closed-loop transfer function of the system, $T_2(s)$, is expressed in Equation (29).

$$T_2(s) = \frac{K_d \cdot s^{\lambda+\mu} + K_p \cdot s^{\lambda} + K_i}{(\tau) \cdot s^{\lambda+1} + (K_p + 1) \cdot s^{\lambda} + K_d \cdot s^{\lambda+\mu} + K_i} \tag{29}$$

In addition to the classical PID structure, the FOPID controller defines the integral and derivative actions in fractional orders, thereby providing a more flexible control structure. The fractional orders, $\lambda = 0.8$ and $\mu = 0.6$, were selected through an experimental scanning method by testing different parameter combinations. Similar to the PID controller, the characteristic equation of the system for the FOPID structure was reformulated. Considering the terms $s^{\lambda+1}$, s^{λ}, and $s^{\lambda+\mu}$ in the denominator of Equation (29), pole placement was performed. The expressions s^{λ}, $s^{\lambda+\mu}$, and $s^{\lambda+1}$ are presented in analytical form in Equation (30).

$$\begin{aligned} s^{\lambda} &= s^{0.8} = -0.9137 + j2.8905 \\ s^{\lambda+\mu} &= s^{1.4} = -6.8932 - j0.9931 \\ s^{\lambda+1} &= s^{1.8} = -5.6986 - j10.697 \end{aligned} \tag{30}$$

The characteristic equation was separated into its real and imaginary components, and these expressions were obtained in terms of K_i in Equations (31) and (32), respectively. The parameters were determined in line with the target transient response.

$$K_d = 0.138751K_i - 0.390635 \tag{31}$$

$$K_p = 0.04767K_i + 0.0137074 \tag{32}$$

Both sets of controller parameters were calculated using the pole placement approach based on reference model matching, and the resulting controller coefficients are given in Table 2.

Table 2. PID and FOPID controller parameters (authors' own work).

Control Type	K_p	K_i	K_d	λ	μ
PID	4.6	16	0.69	1	1
FOPID	0.7764	16	1.8294	0.8	0.6

3.4. Model Validation and Performance Metrics

In this study, model validation is based on a comparative analysis of different controller architectures under the same system model, using various scenarios and quantitative performance metrics. In this context, controller performance was evaluated under scenarios involving storage, no storage, load change, and disturbances. To quantitatively compare controller performances, performance metrics defined based on the error signal and the dynamic energy price signal were used. In error-based evaluation, ISE, ITAE, and RMSE were used, while in price-based analysis, the average unit energy price, standard deviation, and coefficient of variation were considered. These metrics were used to select the most successful controller based on error suppression performance and the impact on price stability. The mathematical expressions used for performance evaluation are presented in Equation (33). ISE is a metric sensitive to large errors. ITAE evaluates the magnitude of the error using a time weight. RMSE indicates the magnitude of the error signal. The average unit price reflects the overall effect of the control structure on the price, while price volatility indicates the fluctuations in the price signal. The coefficient of variation, CV, expresses the magnitude of price volatility relative to the average price. For these metrics, lower values indicate a more successful performance in terms of error suppression, price stability, and overall system performance. The results are presented in graphical and tabular formats. Time series behavior was evaluated through figures, while quantitative metric comparisons were assessed through tables.

$$\begin{aligned} \text{ISE} &= \int e^2(t)dt \\ \text{ITAE} &= \int t\cdot|e(t)|dt \\ \text{RMSE} &= \left(\int \frac{\int e^2(t)dt}{t_{end}-t_{start}}\right)^{1/2} \\ P_{mean} &= \frac{1}{N}\sum_{i=1}^{N} P_i \\ \sigma_P &= \left(\frac{1}{N-1}\sum_{i=1}^{N}(P_i - P_{mean})^2\right)^{1/2} \\ CV &= \frac{\sigma_P}{P_{mean}} \times 100 \end{aligned} \tag{33}$$

Here, $e(t)$ denotes the error, P_i denotes the energy price obtained from the i-th sample, P_{mean} denotes the average energy price, σ_P denotes the standard deviation of the price signal, and N denotes the total number of samples. t_{start} and t_{end} are the start and end times of the analysis period.

4. Simulation Results of Supply–Demand Balancing with Dynamic Price Control

Based on data from Turkey, within the scope of the multi-source simulation study, the total generation and demand data were obtained graphically, and the results are shown in Figure 15. According to the analysis, total generation remains above the demand value. This outcome results from the inclusion of D_S in the simulation to prevent energy shortages and from avoiding deviations of the error signal from zero.

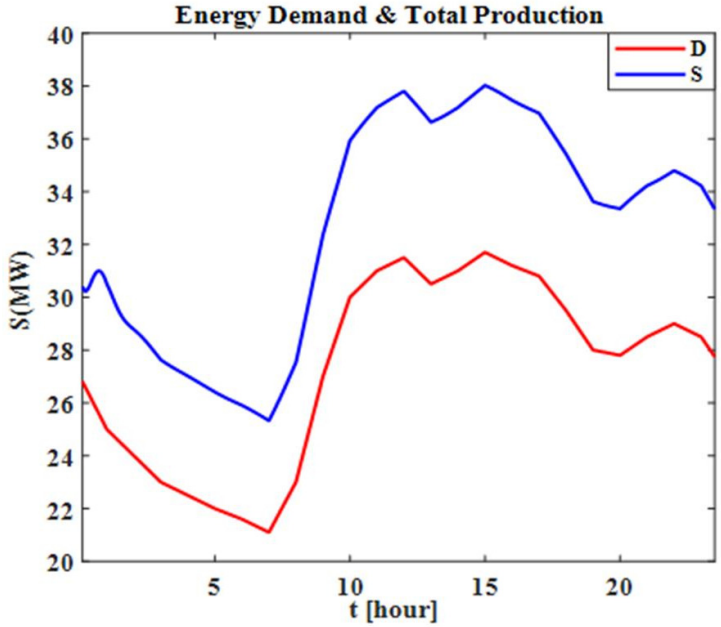


Figure 15. Energy demand-total production model (authors' own work).

4.1. Comparative Analysis of the Closed-Loop Performance of PID, FOPID, and ANFIS-FOPID Controllers

The simulations conducted for supply–demand balancing in a 53 MW system with a multi-source generation infrastructure were designed to examine system performance under variable demand profiles using different controllers. In the generation model, solar, wind, thermal, hydro, and tidal sources were included, while on the demand side, a time-dependent load profile was applied. In closed-loop dynamic energy price control, the PID, FOPID, and ANFIS-FOPID controllers were tested sequentially. The PID and FOPID controller coefficients were used with the values calculated in Table 2, whereas for ANFIS-FOPID, the FOPID coefficients were optimized.

First, for the scenario without storage, the dynamic energy price signals corresponding to the PID, FOPID, and ANFIS-FOPID controllers are presented in Figure 16. Figure 16a shows the general price profile over one day, while Figure 16b provides a zoomed-in view of the critical time window between the 11th and 14th hours for more detailed analysis. This allows a clearer comparison of the results.

Scenario 1;

As seen in Figure 16a, all controllers started the day at the same price level. However, the ANFIS-FOPID controller showed a faster price decrease compared with the others. In the later hours of the day, ANFIS-FOPID stood out with a more pronounced reduction in price. In addition, it limited peak values, thereby reducing energy price fluctuations. While PID and FOPID controllers exhibited similar performance in Figure 16a, a noticeable difference appears in Figure 16b. Due to its fractional coefficient tuning, the FOPID controller provided a better system response than PID. Nevertheless, in the examined scenario, ANFIS-FOPID demonstrated the best performance in terms of ensuring price stability, reducing oscillations, and maintaining the lowest price. Figure 16b shows a zoomed view of the 11th–14th hour interval. Although PID and FOPID displayed comparable price performance, ANFIS-FOPID clearly maintained the lowest price level within stability limits.

Figure 17 represents the ratio of surplus supply to demand. All three controllers prevented energy shortages by keeping the S/D ratio above one across all time intervals. The ANFIS-FOPID controller, however, maintained this ratio at lower levels compared

with the others, thereby reducing surplus generation. This outcome shows that it optimizes resource utilization and indicates the potential to lower energy costs.

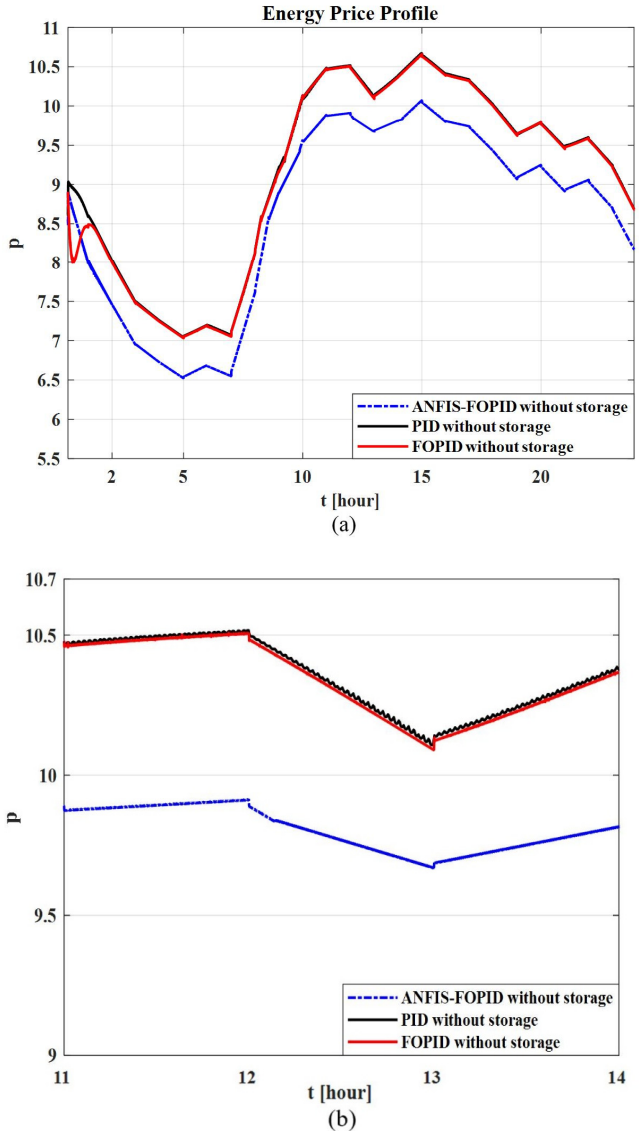


Figure 16. Dynamic energy price profile without energy storage: (**a**) 24 h change in energy prices; (**b**) detailed representation of the energy price signal between hours 11 and 14 (authors' own work).

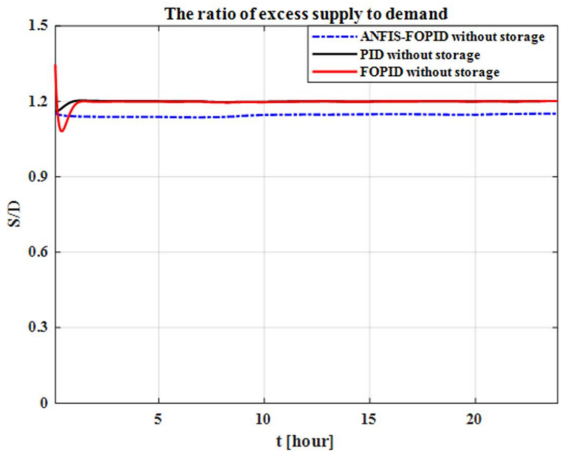


Figure 17. Ratio of excess supply to demand (authors' own work).

In Figure 18, virtual storage is modeled with a time-varying profile over the course of the day. This profile is used to represent battery-like charging and discharging behavior. Such a representation provides a more flexible structure for examining the effects of virtual storage support on the system response.

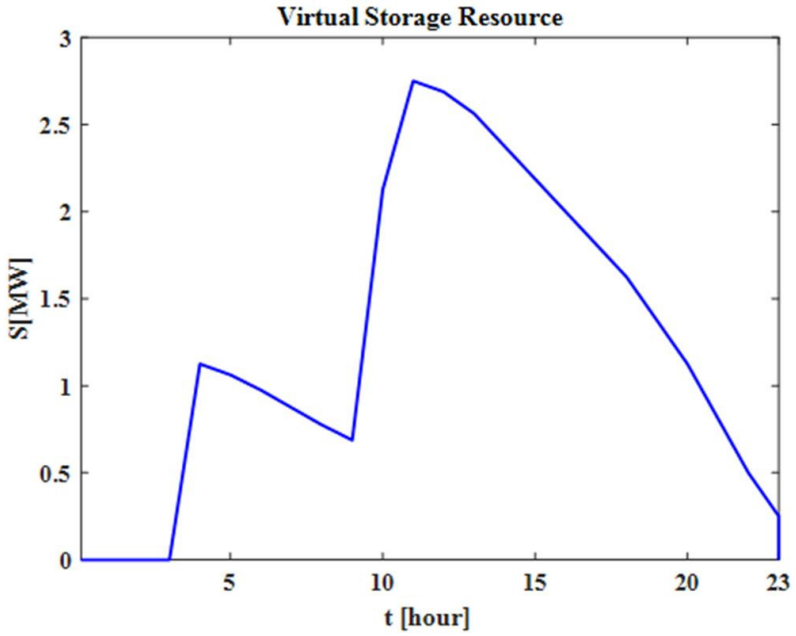


Figure 18. Virtual energy storage (authors' own work).

Figure 19 shows the dynamic energy price signals of the PID, FOPID, and ANFIS-FOPID controllers for the second scenario, where storage was added. The storage unit was integrated into the system as an additional source. With the inclusion of storage, the energy price signals for all controllers decreased, leading to a more stable price balance.

Scenario 2;

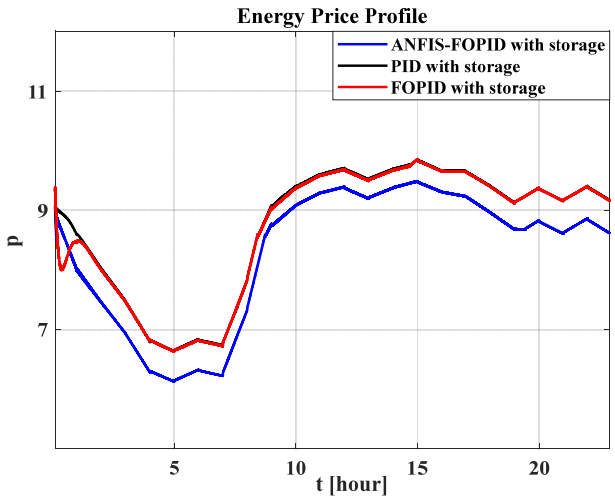


Figure 19. Dynamic energy price profile with energy storage (authors' own work).

Figure 19 presents the energy price profiles obtained when the storage unit is integrated into the system. The ANFIS-FOPID controller produced a lower and more regular price profile throughout the examined time interval. In contrast, the price level remained higher under the PID and FOPID controllers. This result indicates that, in the storage-based configuration, the ANFIS-FOPID controller achieves superior price regulation performance.

In Figure 19, a general downward trend in energy prices was observed following the integration of the virtual storage unit. The price curve provided by the ANFIS-FOPID controller remained at a lower level than the curves of the other controllers throughout the entire 24 h period. When comparing the signals in Figures 16a and 19, which show the scenarios without and with storage, respectively, the price-reducing effect of storage is clearly evident. In both scenarios, the ANFIS-FOPID controller exhibited the lowest price characteristics. Figure 19 demonstrates the effectiveness of storage technologies in ensuring price stability in energy markets with concrete data. The integration of storage has reduced the average energy price compared to the scenario without storage.

To compare the controller performances under storage and non-storage scenarios, error- and price-based performance criteria are presented in Table 3.

Table 3. Comparison of controller performance under with storage and without storage on error indices, price volatility, and average unit energy price (authors' own work).

Controller Type	PID		FOPID		ANFIS-FOPID	
Scenario	**Without Storage**	**With Storage**	**Without Storage**	**With Storage**	**Without Storage**	**With Storage**
ISE	0.82688	0.82594	0.59005	0.58978	0.02247	0.02152
ITAE	4.97359	4.11756	1.69479	1.55452	8.91217	8.71129
RMSE	0.18961	0.18950	0.156798	0.156763	0.03059	0.02994
Price volatility (σ_P)	1.53375	1.32947	1.19849	1.02055	1.12399	0.98271
CV (%)	16.68855	14.91541	13.13336	11.60170	12.78158	11.39915
Average Unit Energy Price	9.19043	8.91343	9.12550	8.79652	8.79384	8.62086

The results presented in Table 3 provide a quantitative basis for evaluating the error reduction capability of the controllers and their effects on the price signal under both storage and non-storage scenarios. The error-based criteria, namely ISE, ITAE, and RMSE, indicate that lower values correspond to more effective error suppression. Lower price volatility and a lower average price reflect a more stable pricing structure. The ANFIS-FOPID controller exhibited the most favorable overall performance in terms of ISE, RMSE, price volatility, and average unit energy price. On the other hand, the low ITAE value of the FOPID controller indicates that it reduced the time-weighted error more effectively in the later stage of the response. When all performance criteria are considered together, it is evident that the ANFIS-FOPID controller provides superior overall performance in terms of system behavior and price stability.

4.2. Robustness Analysis Under Load Variation and Disturbance Scenarios

In this section, the performances of the controllers against sudden demand variations are first evaluated. In this context, peak and dip type disturbances are applied to the demand curve at specific time intervals. In response, the resulting dynamic energy price signal, the variation in the generation profiles of renewable energy sources, and the quantitative performances of the controllers in suppressing the error are examined and compared in detail. Figure 20 shows the peak and dip points imposed on the demand curve at 16:00 and 21:00, respectively.

Scenario 3: Evaluation of Controller Performance under Load Variation

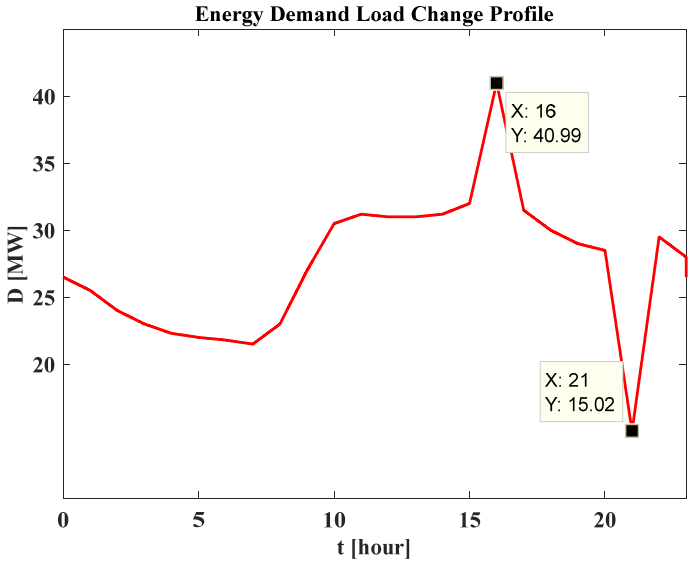


Figure 20. Demand profile with peak and dip perturbations (authors' own work).

Figure 21 illustrates the dynamic response of generation sources to the sudden peak and dip changes introduced into the demand profile. The peak point in the demand profile affected the hydraulic source most significantly among the generation resources. This source rapidly increased its generation profile and contributed to maintaining system balance. While solar, wind, and tidal sources exhibited limited variations within their operating ranges, the thermal source provided stable generation and formed a fundamental support on the supply side. With the sudden dip in demand, a similar adaptation was observed in the generation levels of the producers. In this context, the most noticeable decrease again occurred in the output of the hydraulic source. This clearly demonstrates that producers have flexible generation capabilities in response to problems arising from load variations on the consumer side. Despite the sudden decreases and increases, the share of generation supplied by renewable energy sources was reallocated accordingly.

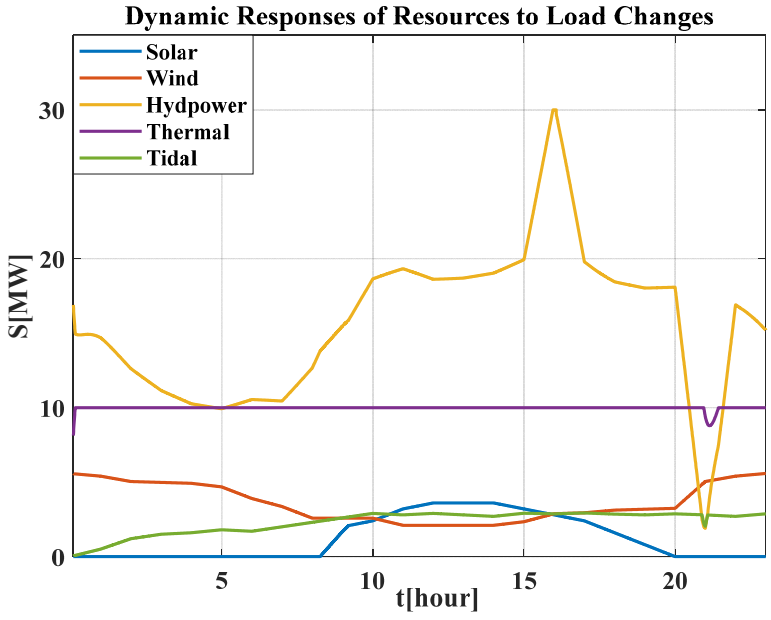


Figure 21. Dynamic Responses of Renewable Energy Sources to Load Changes (authors' own work).

Figure 22a shows the dynamic price responses of different controllers to the sudden peak and dip profile in demand. All controllers generated price signals sensitive to load variations; however, their transient behaviors differed at 16:00 and 21:00, when abrupt load changes occurred. Figure 22b presents a magnified view of the dynamic price signals in the region where the demand exhibits a sudden peak, whereas Figure 22c shows the enlarged view of the region where the demand exhibits a sudden dip. Accordingly, the FOPID controller produced the highest and lowest price signals, while the PID controller exhibited a similar trend but remained more limited compared to the FOPID controller. The ANFIS-FOPID controller displayed a smoother and more controlled increase and decrease profiles in both the peak and dip regions. The results indicate that the ANFIS-FOPID controller provides a balanced structure in terms of continuity and stability of the dynamic price signal under load variations, whereas the FOPID controller exhibits a more aggressive response.

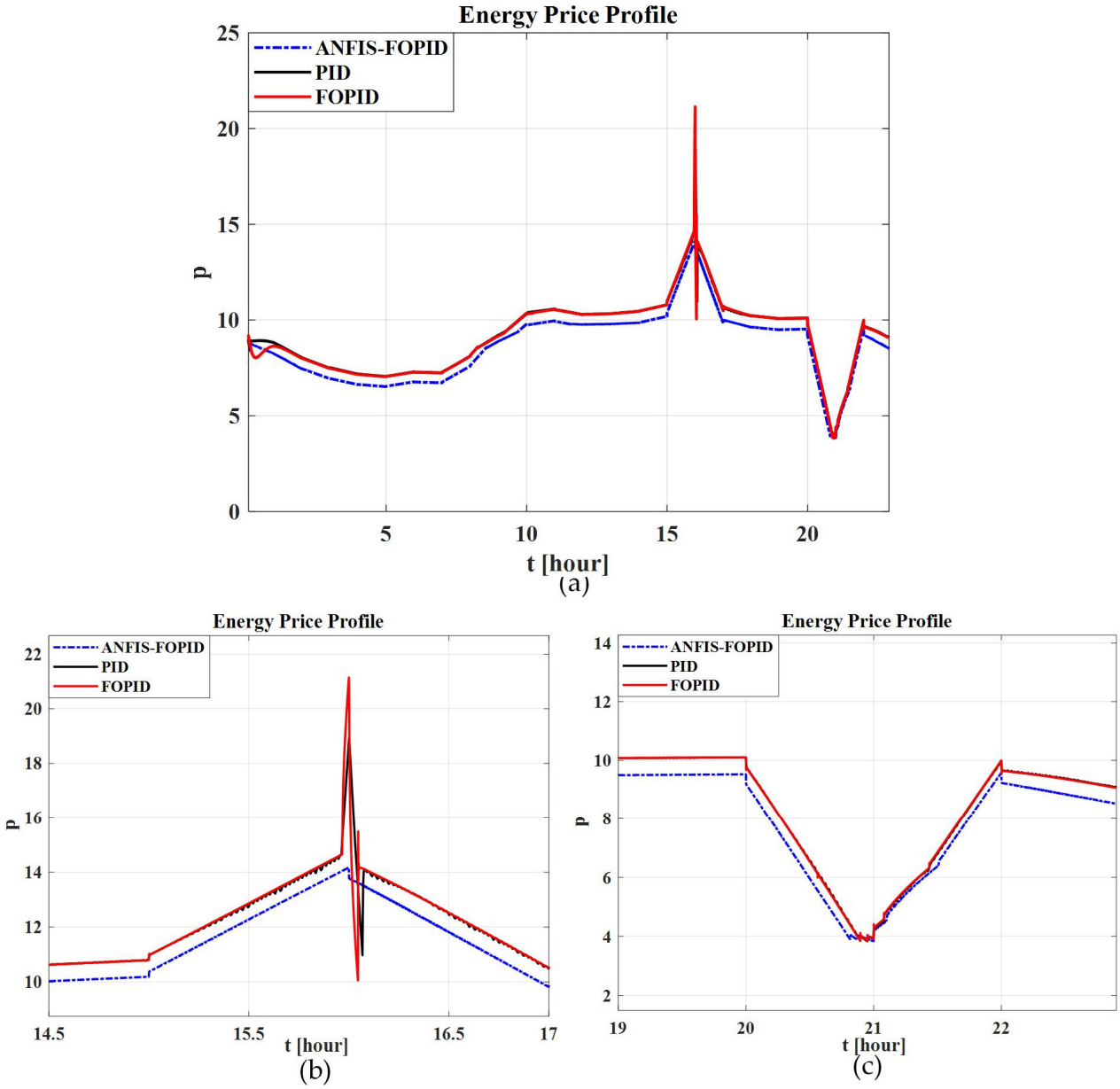


Figure 22. Comparison of Dynamic Energy Price Responses of Controllers to Load Changes: (**a**) 24 h change in energy prices. (**b**,**c**) Detailed representation of the energy price signal peak and dip region (authors' own work).

Table 4 presents the quantitative performance of the controllers examined in response to demand variation in terms of error and price signals. Having the lowest values across all evaluation criteria, the ANFIS-FOPID controller demonstrates superior performance compared with the PID and FOPID controllers in terms of error suppression, price stability, and average price level.

Table 4. Quantitative performance comparison of controllers under load variations (authors' own work).

Control Type	ISE	ITAE	RMSE	σ_P	Average Unit Energy Price	CV (%)
PID	10.1202	25.0046	0.2207	2.0671	9.1607	22.5645
FOPID	9.125	8.5756	0.1660	1.8828	9.1548	20.5665
ANFIS-FOPID	8.792	8.3878	0.0307	1.71503	8.9492	19.1641

Scenario 4: Investigation of Price Signal-Based Controller Performance under Disturbance

In this section, the performances of the controllers against disturbances applied to the price signal are examined. For this purpose, a time-varying disturbance input is imposed on the price signal during specific time intervals. The stabilities of the PID, FOPID, and ANFIS-FOPID controllers are comparatively evaluated over the interval in which the disturbance is applied. Figure 23 shows the disturbance imposed on the price signal between 5:00 and 10:00, while Figure 24 presents the dynamic energy price responses of the different controllers during the disturbance interval.

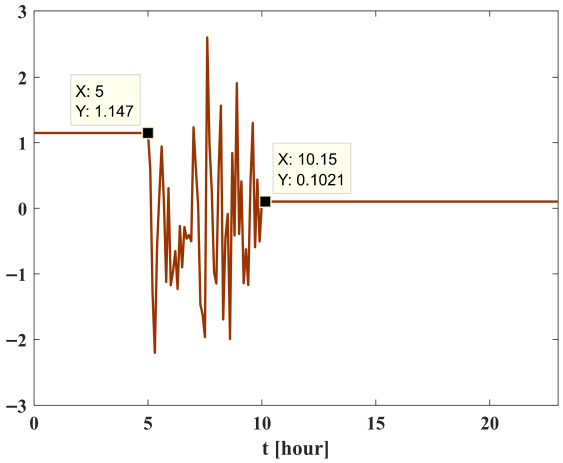


Figure 23. Disturbance Profile Applied to the Price Signal (authors' own work).

Figure 24a shows the energy price responses of the controllers under disturbance over the entire time interval. Significant differences emerged among the controllers during the period in which the disturbance occurred. As shown in Figure 24b, the price signal of the PID controller contains more irregular and higher-amplitude fluctuations. In comparison, the FOPID controller produced a smoother response. The controller that exhibited the most balanced dynamic price signal in terms of both amplitude and stability was the ANFIS-FOPID controller. As a result, under the effect of price disturbance, the ANFIS-FOPID controller demonstrated more stable price behavior than the PID and FOPID controllers.

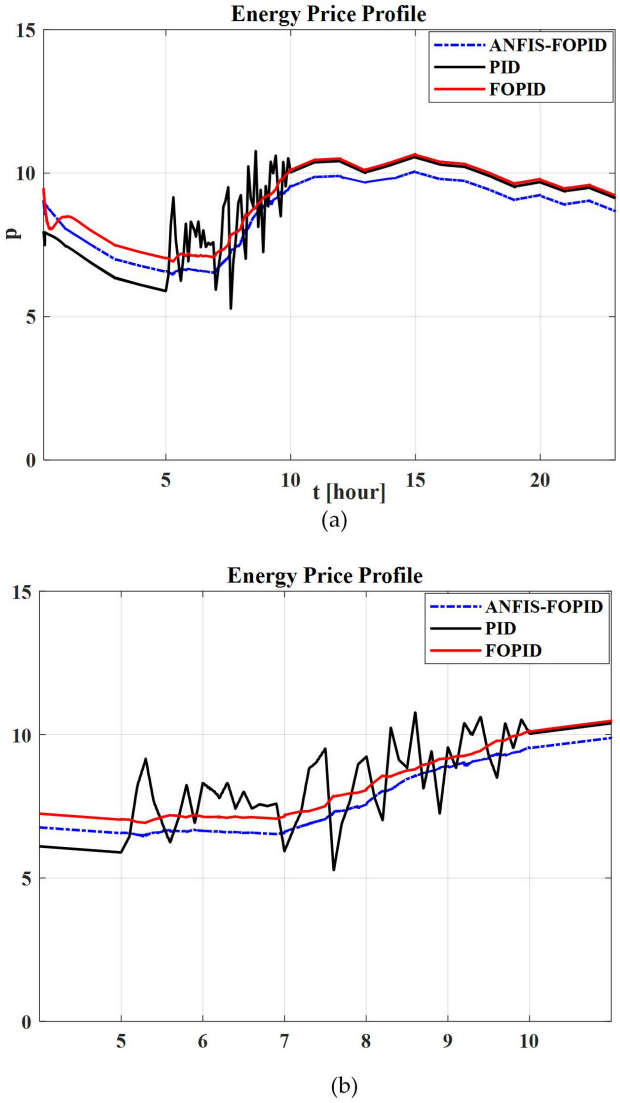


Figure 24. Dynamic Price Responses of the Controllers under Disturbance: (**a**) Energy Price Profile over the Entire Time Interval; (**b**) Enlarged View of the Critical Time Interval in Which the Disturbance Is Applied (authors' own work).

5. Results and Discussion

The findings of this study demonstrate that controller selection in closed-loop dynamic energy pricing systems affects not only the stability of the price signal and the degree to which supply–demand balance is maintained, but also error suppression performance. The study conducted to evaluate the performance of the proposed method consists of several scenarios. In the virtual storage-free scenario, it is observed that the ANFIS-FOPID controller produces lower price levels throughout the day and exhibits less fluctuation compared to PID and FOPID controllers, particularly during time intervals when the load increases. This indicates that the ANFIS-based trained controller parameters, combined with a fractional-order structure, can manage the price signal more effectively. The ANFIS-FOPID controller also demonstrated overall superiority in quantitative performance metrics. It achieved the lowest values in error and price performance evaluation metrics such as ISE, RMSE, average unit energy price, price volatility, and coefficient of variation. This finding indicates that the ANFIS-FOPID controller can establish a relationship between error reduction and price stability. In the same scenario, the low ITAE value of the FOPID controller suggests that low-amplitude, persistent errors can be better suppressed as time progresses. The ANFIS-FOPID controller has successfully suppressed the total error

magnitude and the dynamic energy price signal more effectively than the other controllers. In the scenario where virtual storage was added, the average unit energy price and price volatility decreased for all controllers. However, the lowest quantitative metrics were again achieved with the ANFIS-FOPID controller. This indicates that the use of virtual storage is only feasible with appropriate controller selection. In particular, with the ANFIS-FOPID controller and the virtual storage implemented with a profile that varies throughout the day, the price curve presented a more balanced structure with less pronounced peaks. This result aligns with the concept of providing flexibility in smart grid studies where storage support is present. At the same time, this study expands upon existing research by focusing not only on flexible structure and price stability but also on multiple performance metrics. The load variation scenario exhibited a similar trend. Sudden peaks and dips in the demand curve caused noticeable changes in the price signal. At the same time, renewable energy sources demonstrated a flexible profile to maintain system balance in response to load variations. The results obtained demonstrate that the ANFIS-FOPID controller is resilient to system changes such as sudden load variations. The results obtained under direct disruptive effects applied to the price signal clearly demonstrate the robustness levels of the controllers. While the PID controller generated pronounced and irregular oscillations in the price signal, the FOPID controller caused more limited transient spikes due to its fractional-order advantage. The ANFIS-FOPID controller, on the other hand, produced a more stable and lower-amplitude price response. This indicates that adjusting the parameters of the ANFIS-based controller under the disruptive effect improves system behavior. In particular, the avoidance of generating an erratic price signal under any disruptive influence is significant for the applicability of ANFIS-based dynamic pricing systems. The advantages of controller behaviors that produce more stable responses become evident. This implies both a predictable operational structure on the producer side and a more balanced and stable price response on the consumer side. When reviewing the literature on PID and FOPID studies, it is an expected outcome that the FOPID controller produces better transient performance due to its flexible parameter space. In this study, it is clearly observed that the ANFIS-supported FOPID structure takes the flexible parameter tuning to a higher level.

6. Conclusions

The performance of PID, FOPID, and ANFIS-FOPID controllers in a closed-loop dynamic energy pricing framework was evaluated under multiple operating scenarios. The results show that the ANFIS-FOPID controller provides the most balanced overall performance in terms of error suppression and price volatility reduction. A key contribution of the study is the comparative assessment of controller behavior under storage, disturbance, and load variation scenarios by using both error-based and price-based quantitative metrics. The analyses were conducted through simulation using 24 h data. Therefore, the results are limited to daily supply and demand profiles under the selected simulation conditions. Seasonal variations and real-time market dynamics may lead to different system responses in practical applications. However, the main scope of the study is the comparative evaluation of dynamic energy price responses under different controller structures. In this respect, the proposed method offers a flexible structure that can be extended to different datasets and operating conditions. Future studies may consider seasonal data, economic crisis conditions, and real-time market environments. The proposed approach may support price stability in smart grids and the implementation of flexible energy management strategies.

Author Contributions: Conceptualization, Z.Y., A.K. and Ö.Ö.; methodology, Z.Y. and S.G.K.; software, Ö.Ö. and Z.Y.; validation, Z.Y., Ö.Ö. and A.K.; formal analysis, Z.Y. and S.G.K.; investigation, Z.Y.; resources, Z.Y., Ö.Ö. and A.K.; data curation, Ö.Ö., Z.Y. and S.G.K.; writing—original draft preparation, Z.Y.; writing—review and editing, Z.Y., Ö.Ö., A.K. and S.G.K.; visualization, S.G.K.; supervision, A.K., Ö.Ö.; project administration, A.K. All authors have read and agreed to the published version of the manuscript.

Funding: This work was supported by the Inonu University Scientific Research Projects Coordination Unit (Project No. FBA-2026-4747).

Data Availability Statement: The raw data supporting the conclusions of this article will be made available by the authors upon request.

Conflicts of Interest: The authors declare no conflicts of interest.

References

1. Khalid, M. Smart Grids and Renewable Energy Systems: Perspectives and Grid Integration Challenges. *Energy Strategy Rev.* **2024**, *51*, 101299. [CrossRef]
2. Stephens, J.C.; Wilson, E.J.; Peterson, T.R.; Meadowcroft, J. Getting Smart? Climate Change and the Electric Grid. *Challenges* **2013**, *4*, 201–216. [CrossRef]
3. Tanrıöven, K.; Yararbaş, S.; Cengiz, H. Smart Grid, the Future Electricity Distribution Network. In *Proceedings of the Electrical-Electronics and Computer Symposium, Elazig, Turkey, 9–11 June 2011*; Fırat University: Elazig, Turkey, 2011; pp. 52–55.
4. Sun, Q.; Ge, X.; Liu, L.; Xu, X.; Zhang, Y.; Niu, R.; Zeng, Y. Review of Smart Grid Comprehensive Assessment Systems. *Energy Procedia* **2011**, *12*, 219–229. [CrossRef]
5. Kabalci, Y. A Survey on Smart Metering and Smart Grid Communication. *Renew. Sustain. Energy Rev.* **2016**, *57*, 302–318. [CrossRef]
6. Alagöz, B.B. Energy Balancing in Smard Grids Under Varying Generation and Demand Conditions. Ph.D. Thesis, Inonu University, Institute of Science, Malatya, Turkey, 2015.
7. Alagöz, B.B.; Kaygusuz, A. Dynamic Energy Price Control with Closed Loop Fractional Order PI Controller and Automatic Energy Supply-Demand Balancing Application in Smart Grids. In *Proceedings of the TOK, Kocaeli, Turkey, 11–13 September 2014*; Kocaeli University: Kocaeli, Turkey, 2014; pp. 535–539.
8. Yalçınöz, Z.; Kaygusuz, A. Dynamic Price Control Using Pole Placement Method in Smart Grids. *Comput. Sci.* **2021**, *IDAP-2021*, 411–421. [CrossRef]
9. Tan, K.M.; Babu, T.S.; Ramachandaramurthy, V.K.; Kasinathan, P.; Solanki, S.G.; Raveendran, S.K. Empowering Smart Grid: A Comprehensive Review of Energy Storage Technology and Application with Renewable Energy Integration. *J. Energy Storage* **2021**, *39*, 102591. [CrossRef]
10. Ah-voun, D.; Chyong, C.K.; Li, C. Europe's Energy Security: From Russian Dependence to Renewable Reliance. *Energy Policy* **2024**, *184*, 113856. [CrossRef]
11. Guarascio, D.; Reljic, J.; Zezza, F. Energy Vulnerability and Resilience in the EU: Concepts, Empirics and Policy. *J. Ind. Bus. Econ.* **2025**, *52*, 683–726. [CrossRef]
12. Kim, J.; Jaumotte, F.; Panton, A.J.; Schwerhoff, G. Energy Security and the Green Transition. *Energy Policy* **2025**, *198*, 114409. [CrossRef]
13. Iglinski, B.; Kiełkowska, U.; Mazurek, K.; Druzynski, S.; Pietrzak, M.B.; Kumar, G.; Skrzatek, M.; Zinecker, M.; Veeramuthu, A.; Piechota, G. Renewable Energy Transition in Europe in the Context of Renewable Energy Transition Processes in the World. A Review. *Heliyon* **2024**, *10*, e40997. [CrossRef] [PubMed]
14. Kallel, R.; Boukettaya, G.; Krichen, L. Control Management Strategy of Stand-Alone Hybrid Power Micro-System Using Super-Capacitor. *Int. J. Renew. Energy Res.* **2014**, *4*, 210–223.
15. Peterson, R.B. A Concept for Storing Utility-Scale Electrical Energy in the Form of Latent Heat. *Energy* **2011**, *36*, 6098–6109. [CrossRef]
16. Kang, W.; Chen, M.; Lai, W.; Luo, Y. Distributed Real-Time Power Management for Virtual Energy Storage Systems Using Dynamic Price. *Energy* **2021**, *216*, 119069. [CrossRef]
17. Chong, L.W.; Wong, Y.W.; Rajkumar, R.K.; Rajkumar, R.K.; Isa, D. Hybrid Energy Storage Systems and Control Strategies for Stand-Alone Renewable Energy Power Systems. *Renew. Sustain. Energy Rev.* **2016**, *66*, 174–189. [CrossRef]
18. Psarros, G.N.; Dratsas, P.A.; Chinaris, P.P.; Papathanassiou, S.A. Assessing the Implications of RES Technology Mix on Curtailments, Storage Requirements and System Economics. *Appl. Energy* **2025**, *381*, 125159. [CrossRef]
19. TEİAŞ. *TEİAŞ Üretim Kapasite Projeksiyonu 2021–2025*; Turkish Electricity Transmission Corporation: Ankara, Turkey, 2021. Available online: https://www.epdk.gov.tr/Detay/Icerik/3-0-66/elektrikuretim-kapasite-projeksiyonlari (accessed on 15 April 2026).

20. Khan, A.R.; Mahmood, A.; Safdar, A.; Khan, Z.A.; Khan, N.A. Load Forecasting, Dynamic Pricing and DSM in Smart Grid: A Review. *Renew. Sustain. Energy Rev.* **2016**, *54*, 1311–1322. [CrossRef]
21. Chakraborty, S.; Ito, T.; Senjyu, T. Smart Pricing Scheme: A Multi-Layered Scoring Rule Application. *Expert Syst. Appl.* **2014**, *41*, 3726–3735. [CrossRef]
22. Kaygusuz, A. Closed Loop Elastic Demand Control by Dynamic Energy Pricing in Smart Grids. *Energy* **2019**, *176*, 596–603. [CrossRef]
23. Parvania, M.; Fotuhi-Firuzabad, M. Demand Response Scheduling by Stochastic SCUC. *IEEE Trans. Smart Grid* **2010**, *1*, 89–98. [CrossRef]
24. He, Y.; Pang, Y.; Guan, J. A TOU Pricing Mechanism to Promote Renewable Energy Consumption: The Case of the Western Inner Mongolia Grid in China. *Math. Probl. Eng.* **2017**, *2017*, 9545358. [CrossRef]
25. Pallonetto, F.; Oxizidis, S.; Milano, F.; Finn, D. The Effect of Time-of-Use Tariffs on the Demand Response Flexibility of an All-Electric Smart-Grid-Ready Dwelling. *Energy Build.* **2016**, *128*, 56–67. [CrossRef]
26. Rahman, M.M.; Hettiwatte, S.; Shafiullah, G.M.; Arefi, A. An Analysis of the Time of Use Electricity Price in the Residential Sector of Bangladesh. *Energy Strategy Rev.* **2017**, *18*, 183–198. [CrossRef]
27. Wang, J.; Bloyd, C.N.; Hu, Z.; Tan, Z. Demand Response in China. *Energy* **2010**, *35*, 1592–1597. [CrossRef]
28. Yang, Y.; Wang, M.; Liu, Y.; Zhang, L. Peak-off-Peak Load Shifting: Are Public Willing to Accept the Peak and off-Peak Time of Use Electricity Price? *J. Clean. Prod.* **2018**, *199*, 1066–1071. [CrossRef]
29. Zhou, K.; Wei, S.; Yang, S. Time-of-Use Pricing Model Based on Power Supply Chain for User-Side Microgrid. *Appl. Energy* **2019**, *248*, 35–43. [CrossRef]
30. Gyamfi, S.; Krumdieck, S.; Urmee, T. Residential Peak Electricity Demand Response—Highlights of Some Behavioural Issues. *Renew. Sustain. Energy Rev.* **2013**, *25*, 71–77. [CrossRef]
31. Shewale, A.; Mokhade, A.; Lipare, A.; Bokde, N.D. Efficient Techniques for Residential Appliances Scheduling in Smart Homes for Energy Management Using Multiple Knapsack Problem. *Arab. J. Sci. Eng.* **2024**, *49*, 3793–3813. [CrossRef]
32. Yan, X.; Ozturk, Y.; Hu, Z.; Song, Y. A Review on Price-Driven Residential Demand Response. *Renew. Sustain. Energy Rev.* **2018**, *96*, 411–419. [CrossRef]
33. Park, S.C.; Jin, Y.G.; Song, H.Y.; Yoon, Y.T. Designing a Critical Peak Pricing Scheme for the profit Maximization Objective Considering Price Responsiveness of Customers. *Energy* **2015**, *83*, 521–531. [CrossRef]
34. Boom, A.; Schwenen, S. Is Real-Time Pricing Smart for Consumers? *J. Regul. Econ.* **2021**, *60*, 193–213. [CrossRef]
35. Duan, Q. A Price-Based Demand Response Scheduling Model in Day-Ahead Electricity Market. In *Proceedings of the IEEE Power and Energy Society General Meeting (PESGM), Boston, MA, USA, 17–21 July 2016*; IEEE: Piscataway, NJ, USA, 2016; pp. 1–5.
36. Danxi, L.; Bo, Z.; Yan, Q.; Xu, Y. Optimal Control Model of Electric Vehicle Demand Response Based on Real—Time Electricity Price. In *Proceedings of the IEEE 2nd Information Technology, Networking, Electronic and Automation Control Conference (ITNEC), Chengdu, China, 15–17 December 2017*; IEEE: Piscataway, NJ, USA, 2017; pp. 1815–1818.
37. He, S.; Wallace, M.; Wilson, C.; Liebman, A. Fast Electrical Demand Optimization Under Real-Time Pricing. In Proceedings of the AAAI Conference on Artificial Intelligence, San Francisco, CA, USA, 4–9 February 2017. [CrossRef]
38. Alquthami, T.; Milyani, A.H.; Awais, M.; Rasheed, M.B. An Incentive Based Dynamic Pricing in Smart Grid: A Customer's Perspective. *Sustainability* **2021**, *13*, 6066. [CrossRef]
39. Dutta, G.; Mitra, K. A Literature Review on Dynamic Pricing of Electricity. *J. Oper. Res. Soc.* **2017**, *68*, 1131–1145. [CrossRef]
40. Dursun, E.; Siano, P. A Dynamic Pricing Model for Turkey's Electricity Distribution Companies in the Future Smart Grid Infrastructure. In *Proceedings of the Innovations in Intelligent Systems and Applications Conference, ASYU, Izmir, Turkey, 31 October–2 November 2019*; IEEE: Piscataway, NJ, USA, 2019; pp. 1–5.
41. Khattak, H.A.; Tehreem, K.; Almogren, A.; Ameer, Z.; Din, I.U.; Adnan, M. Dynamic Pricing in Industrial Internet of Things: Blockchain Application for Energy Management in Smart Cities. *J. Inf. Secur. Appl.* **2020**, *55*, 102615. [CrossRef]
42. Ahmed, R.; Amer, M. A Hardware Dynamic Pricing Based Energy Management System. In *Proceedings of the 4th International Conference on Power Electronics and their Applications, ICPEA, Elazig, Turkey, 25–27 September 2019*; IEEE: Piscataway, NJ, USA, 2019; pp. 1–5.
43. Anand, H.; Ramasubbu, R. A Real Time Pricing Strategy for Remote Micro-Grid with Economic Emission Dispatch and Stochastic Renewable Energy Sources. *Renew. Energy* **2018**, *127*, 779–789. [CrossRef]
44. Bukhsh, W.; Zhang, C.; Pinson, P. An Integrated Multiperiod OPF Model with Demand Response and Renewable Generation Uncertainty. *IEEE Trans. Smart Grid* **2015**, *7*, 1495–1503. [CrossRef]
45. Giorgio, A.D.; Liberati, F.; Lanna, A. Real Time Optimal Power Flow Integrating Large Scale Storage Devices and Wind Generation. In Proceedings of the 2015 23rd Mediterranean Conference on Control and Automation (MED), Torremolinos, Spain, 16–19 June 2015. [CrossRef]
46. Zhang, D.; Du, T.; Yin, H.; Xia, S.; Zhang, H. Multi-Time-Scale Coordinated Operation of a Combined System with Wind-Solar-Thermal-Hydro Power and Battery Units. *Appl. Sci.* **2019**, *9*, 3574. [CrossRef]

47. Hill, C.A.; Such, M.C.; Chen, D.; Gonzalez, J.; Grady, W.M.K. Battery Energy Storage for Enabling Integration of Distributed Solar Power Generation. *IEEE Trans. Smart Grid* **2012**, *3*, 850–857. [CrossRef]
48. Owais, S.; Shohan, M.J.A.; Islam, M.M.; Faruque, M.O. Management of Grid Connected Energy Storage Systems Employing Real-Time Energy Price. *J. Energy Storage* **2024**, *92*, 112097. [CrossRef]
49. Hark, C.; Uçkan, T.; Karcı, A. A New Multi-Document Summarisation Approach Using Saplings Growing-up Optimisation Algorithms: Simultaneously Optimised Coverage and Diversity. *J. Inf. Sci.* **2024**, *50*, 635–650. [CrossRef]
50. Gülmez, B. A New Multi-Objective Hyperparameter Optimization Algorithm for COVID-19 Detection from X-Ray Images. *Soft Comput.* **2024**, *28*, 11601–11617. [CrossRef]
51. Akter, A.; Zafir, E.I.; Dana, N.H.; Joysoyal, R.; Sarker, S.K.; Li, L.; Muyeen, S.M.; Das, S.K.; Kamwa, I. A Review on Microgrid Optimization with Meta-Heuristic Techniques: Scopes, Trends and Recommendation. *Energy Strategy Rev.* **2024**, *51*, 101298. [CrossRef]
52. Upadhaya, D.; Biswas, S.; Dutta, S.; Bhattacharya, A. Optimal Power Flow and Grid Frequency Control of Conventional and Renewable Energy Source Using Evolutionary Algorithm Based FOPID Controller. *Renew. Energy Focus* **2025**, *53*, 100676. [CrossRef]
53. Sharma, S.K.; Alghamdi, R.; Alasmari, S.; Sharma, N.K.; Khan, H.; Ahmad, F. Fractional Order PID Controllers for Collaborative Energy Management in IoT-Smart Cities: Hybrid Optimization Algorithms for Demand. *Energy Rep.* **2024**, *12*, 5551–5566. [CrossRef]
54. Liu, K.; Li, B.; Jiang, Q.; Zhang, Y.; Liu, T. Fault Ride-Through Strategy for Hybrid Cascaded HVdc Systems Based on Controllable LCC. *IEEE Trans. Circuits Syst. II Express Briefs* **2026**, *73*, 88–92. [CrossRef]
55. Alagoz, B.B.; Kaygusuz, A.; Akcin, M.; Alagoz, S. A Closed-Loop Energy Price Controlling Method for Real-Time Energy Balancing in a Smart Grid Energy Market. *Energy* **2013**, *59*, 95–104. [CrossRef]
56. Khan, T.; Ullah, K.; Hafeez, G.; Khan, I.; Khalid, A.; Shafiq, Z.; Usman, M.; Qazi, A.B. Closed-Loop Elastic Demand Control under Dynamic Pricing Program in Smart Microgrid Using Super. *Sensors* **2020**, *20*, 4376. [CrossRef]
57. Gupta, D.; Goyal, V. An Optimized Fractional Order PID Controller for Integrated Power System. In *Proceedings of the ICICCT 2019—System Reliability, Quality Control, Safety, Maintenance and Management, New Delhi, India, 11 May 2019*; Springer: Singapore, 2019; pp. 663–672.
58. Agwa, A.M.; Abdeen, M.; Shaaban, S.M. Optimal FOPID Controllers for LFC Including Renewables by Bald Eagle Optimizer. *Comput. Mater. Contin.* **2022**, *73*, 5525–5541. [CrossRef]
59. Daraz, A.; Malik, S.A.; Basit, A.; Aslam, S.; Zhang, G. Modified FOPID Controller for Frequency Regulation of a Hybrid Interconnected System of Conventional and Renewable Energy Sources. *Fractal Fract.* **2023**, *7*, 89. [CrossRef]
60. Mukherjee, M.; Banerjee, A. Reactive Power Compensation in Hybrid Energy Systems: FOPID-Controlled UPFC with Modified Osprey Optimization Algorithm. *Int. J. Inf. Technol.* **2024**. [CrossRef]
61. Murugesan, D.; Jagatheesan, K.; Shah, P.; Sekhar, R. Fractional Order $PI^{\lambda}D^{\mu}$ Controller for Microgrid Power System Using Cohort Intelligence Optimization. *Results Control Optim.* **2023**, *11*, 100218. [CrossRef]
62. Reddy, P.; Reddy, M.; Kiran, K.U.; Balaji, D.; Reddy, D.; Kumar, K.S. Smart Micro-Grid Integration with Bidirectional DC Fast Charging: Harnessing Vehicle-to-Grid Technology. *Int. J. Sci. Res. Arch.* **2024**, *13*, 3227–3238. [CrossRef]
63. Islam, M.A.; Singh, J.G.; Jahan, I.; Hossain Lipu, M.S.; Jamal, T.; Elavarasan, R.M.; Mihet-Popa, L. Modeling and Performance Evaluation of ANFIS Controller-Based Bidirectional Power Management Scheme in Plug-in Electric Vehicles Integrated with Electric Grid. *IEEE Access* **2021**, *9*, 166762–166780. [CrossRef]
64. Kandasamy, K.; Renuga, P.; Velu, S.K. ELM-ANFIS Based Controller for Plug-in Electric Vehicle to Grid Integration. *Teh. Vjesn. Tech. Gaz.* **2018**, *25*, 15–22. [CrossRef]
65. Zhao, B.; Xue, M.; Zhang, X.; Wang, C.; Zhao, J. An MAS Based Energy Management System for a Stand-Alone Microgrid at High Altitude. *Appl. Energy* **2015**, *143*, 251–261. [CrossRef]
66. Ning, J.; Hao, S.; Zeng, A.; Chen, B.; Tang, Y. Research on Multi-Timescale Coordinated Method for Source-Grid-Load with Uncertain Renewable Energy Considering Demand Response. *Sustainability* **2021**, *13*, 3400. [CrossRef]
67. Wu, C.; Li, J.; Liu, W.; He, Y.; Nourmohammadi, S. Short-Term Electricity Demand Forecasting Using a Hybrid ANFIS–ELM Network Optimised by an Improved Parasitism–Predation Algorithm. *Appl. Energy* **2023**, *345*, 121316. [CrossRef]
68. Prince; Hati, A.S.; Kumar, P. An Adaptive Neural Fuzzy Interface Structure Optimisation for Prediction of Energy Consumption and Airflow of a Ventilation System. *Appl. Energy* **2023**, *337*, 120879. [CrossRef]
69. Khosravi, A.; Machado, L.; Nunes, R.O. Time-Series Prediction of Wind Speed Using Machine Learning Algorithms: A Case Study Osorio Wind Farm, Brazil. *Appl. Energy* **2018**, *224*, 550–566. [CrossRef]
70. Amadou, B.A.; Ndiaye, A.; Ndiaye, E.h.M.; Mbodji, S. Power Optimization of a Photovoltaic System with Artificial Intelligence Algorithms over Two Seasons in Tropical Area. *MethodsX* **2023**, *10*, 101959. [CrossRef]
71. Anbarasu, E.; Muthu Vijaya Pandian, S.; Basha, A.R. An Improved Power Conditioning System for Grid Integration of Solar Power Using ANFIS Based FOPID Controller. *Microprocess. Microsyst.* **2020**, *74*, 103030. [CrossRef]

72. Panchariya, R.; Syal, P. An Improved Current Control Charging Scheme Using Neuro-Fuzzy and Fopid Based Mppt System for Ev Charging. *Int. J. Eng. Trends Technol.* **2021**, *69*, 251–257. [CrossRef]
73. Golnaraghi, F.; Kuo, B.C. *Automatic Control Systems*, 9th ed.; Wiley: Hoboken, NJ, USA, 2010.
74. Cohen, G.H.; Coon, G.A. Theoretical Consideration of Retarded Control. *Trans. ASME* **1952**, *75*, 827–834. [CrossRef]
75. Ogata, K. *Modern Control Engineering*, 5th ed.; Prentice Hall: Saddle River, NJ, USA, 2002.
76. Ziegler, J.G.; Nichols, N.B. Optimum Settings for Automatic Controllers. *Trans. ASME* **1942**, *64*, 759–765. [CrossRef]
77. Schmid, R.; Ntogramatzidis, L.; Nguyen, T.; Pandey, A. A Unified Method for Optimal Arbitrary Pole Placement. *Automatica* **2014**, *50*, 2150–2154. [CrossRef]
78. Wang, Z.; Liu, X.; Wang, W. Pole Placement Method on a Class of Nonlinear Systems with Adaptive Backstepping Technique. *Int. J. Syst. Sci.* **2022**, *53*, 613–633. [CrossRef]
79. Wang, Q.G.; Zhang, Z.; Astrom, K.J.; Chek, L.S. Guaranteed Dominant Pole Placement with PID Controllers. *J. Process Control* **2009**, *19*, 349–352. [CrossRef]
80. Çakmak, C. Fuzzy Based Optimization Method for Ziegler-Nichols PID Controller Parameters. Master's Thesis, Istanbul Technical University, Institute of Science, Istanbul, Turkey, 2011.
81. Karagözoğlu, L.; Duranay, Z.B. Yapay Sinir Ağları Kullanılarak Fotovoltaik Sistemin Maksimum Güç Noktası Takibi Maximum Power Point Tracking of the Photovoltaic System Using Artificial Neural Networks. *Gümüşhane Üniversitesi Fen Bilim. Derg.* **2023**, *13*, 733–749. [CrossRef]
82. Wang, L.; Liu, J.; Yang, C.; Wu, D. A Novel Interval Dynamic Reliability Computation Approach for the Risk Evaluation of Vibration Active Control Systems Based on PID Controllers. *Appl. Math. Model.* **2021**, *92*, 422–446. [CrossRef]
83. Sumarmad, K.A.A.S.; Sulaiman, N.; Wahab, N.I.A.; Hizam, H. Artificial Neural Networks, PID, and Fuzzy Logic Controllers. *Energies* **2022**, *15*, 303. [CrossRef]
84. Aström, K.J.; Hagglund, T. *PID Controllers: Theory-Design-and Tuning*, 2nd ed.; Instrument Society of America: Research Triangle Park, NC, USA, 1995.
85. Zhang, F.; Yang, C.; Zhou, X.; Gui, W. Fractional-Order PID Controller Tuning Using Continuous State Transition Algorithm. *Neural Comput. Appl.* **2018**, *29*, 795–804. [CrossRef]
86. Prabhakaran, A.; Ponnusamy, T.; Janarthanan, G. Optimized Fractional Order PID Controller with Sensorless Speed Estimation for Torque Control in Induction Motor. *Expert Syst. Appl.* **2025**, *249*, 123574. [CrossRef]
87. Nasir, M.; Khadraoui, S. Fractional-Order PID Controller Design Using PSO and GA. In *Proceedings of the 2021 14th International Conference on Developments in eSystems Engineering (DeSE), Sharjah, United Arab Emirates, 7–10 December 2021*; IEEE: Piscataway, NJ, USA, 2021; pp. 192–197. [CrossRef]
88. Aseem, K.; Kumar, S.S. Hybrid k—Means Grasshopper Optimization Algorithm Based FOPID Controller with Feed Forward DC—DC Converter for Solar—Wind Generating System. *J. Ambient Intell. Humaniz. Comput.* **2022**, *13*, 2439–2462. [CrossRef]
89. Jain, R.V.; Aware, M.V.; Junghare, A.S. Tuning of Fractional Order PID Controller U Sing Particle Swarm Optimization Technique for DC Motor Speed Control. In *Proceedings of the 2016 IEEE 1st International Conference on Power Electronics, Intelligent Control and Energy Systems (ICPEICES), Delhi, India, 4–6 July 2016*; IEEE: Piscataway, NJ, USA, 2016; pp. 1–4. [CrossRef]
90. Arpaci, H.; Ozguven, O.F. Design of Adaptive Fractional-Order PID Controller to Enhance Robustness by Means of Adaptive Network Fuzzy Inference System. *Int. J. Fuzzy Syst.* **2017**, *19*, 1118–1131. [CrossRef]
91. Petráš, I.; Dorčák, L.; Koštial, I. Control Quality Enhancement by Fractional Order Controllers. *Acta Montan. Slovaca* **1998**, *3*, 143–148.
92. Suriya, L.J.J.; Mano, J.S.C. Enhanced PV Power Optimization: Integrating Jordan Neural Network MPPT with FOPID—Controlled SEPIC Converter for Non—Linear Load Applications. *Opt. Quantum Electron.* **2025**, *57*, 271. [CrossRef]
93. Zhang, Q.; Wang, X.; Fu, M. Optimal Implementation Strategies for Critical Peak Pricing. In *Proceedings of the International Conference on the European Energy Market, Leuven, Belgium, 27–29 May 2009*; IEEE: Piscataway, NJ, USA, 2009; pp. 1–6.
94. Buckley, J.J.; Hayashi, Y. Fuzzy Neural Networks: A Survey. *Fuzzy Sets Syst.* **1994**, *66*, 1–13. [CrossRef]
95. Takagi, T.; Sugeno, M. Fuzzy Identification of Systems and Its Applications to Modeling and Control. *IEEE Trans. Syst. Man Cybern.* **1985**, *15*, 116–132. [CrossRef]
96. Faria, P.; Vale, Z. Demand Response in Electrical Energy Supply: An Optimal Real Time Pricing Approach. *Energy* **2011**, *36*, 5374–5384. [CrossRef]
97. Yalçinöz, Z.; Kaygusuz, A. A Study on Dynamic Energy Pricing in Smart Grids. *Comput. Sci.* **2022**, *IDAP-2022*, 21–31. [CrossRef]

Disclaimer/Publisher's Note: The statements, opinions and data contained in all publications are solely those of the individual author(s) and contributor(s) and not of MDPI and/or the editor(s). MDPI and/or the editor(s) disclaim responsibility for any injury to people or property resulting from any ideas, methods, instructions or products referred to in the content.